

Explaining Globally Inhomogeneous Future Changes in Monsoons Using Simple Moist Energy Diagnostics

RODRIGO J. BOMBARDI^a AND WILLIAM R. BOOS^{b,c}

^a Department of Geography, Texas A&M University, College Station, Texas

^b Department of Earth and Planetary Science, University of California, Berkeley, California

^c Climate and Ecosystem Sciences Division, Lawrence Berkeley National Laboratory, Berkeley, California

(Manuscript received 5 January 2021, in final form 3 August 2021)

ABSTRACT: This study examines the annual cycle of monsoon precipitation simulated by models from phase 6 of the Coupled Model Intercomparison Project (CMIP6), then uses moist energy diagnostics to explain globally inhomogeneous projected future changes. Rainy season characteristics are quantified using a consistent method across the globe. Model bias is shown to include rainy season onsets tens of days later than observed in some monsoon regions (India, Australia, and North America) and overly large summer precipitation in others (North America, South America, and southern Africa). Projected next-century changes include rainy season lengthening in the two largest Northern Hemisphere monsoon regions (South Asia and central Sahel) and shortening in the two largest Southern Hemisphere regions (South America and southern Africa). Changes in the North American and Australian monsoons are less coherent across models. To understand these changes, relative moist static energy (MSE) is defined as the difference between local and tropical-mean surface air MSE. Future changes in relative MSE in each region correlate well with onset and demise date changes. Furthermore, Southern Hemisphere regions projected to undergo rainy season shortening are spanned by an increasing equator-to-pole MSE gradient, suggesting their rainfall will be increasingly inhibited by fluxes of dry extratropical air; Northern Hemisphere regions with projected lengthening of rainy seasons undergo little change in equator-to-pole MSE gradient. Thus, although model biases raise questions as to the reliability of some projections, these results suggest that globally inhomogeneous future changes in monsoon timing may be understood through simple measures of surface air MSE.

KEYWORDS: Monsoons; Climate change; Coupled models; Interannual variability; Seasonal cycle

1. Introduction

Monsoon systems and their variability greatly influence a large fraction of the global human population. Variations in the timing of the start and end of the monsoon season and in seasonal precipitation totals have important consequences for energy generation, agriculture, human health, and property loss (e.g., due to landslides, floods, and fires). Thorough assessment of future projections of the annual cycle of monsoon precipitation is thus of great consequence.

However, the effort to reliably project future monsoon rainfall has been hindered by model bias, incomplete understanding of the mechanisms governing future changes, and the use of disparate methodologies. Here we touch on all of these issues through analysis of the historical and future seasonal cycle of monsoon precipitation simulated by phase 6 of the Coupled Model Intercomparison Project (CMIP6). We assess the characteristics of the wet season (e.g., timing and total wet season precipitation) in core monsoon regions using a consistent approach over all regions, then use simple moist energy diagnostics to frame a hypothesis for the spatial inhomogeneity of the projected changes. Mechanistic hypotheses are important in such assessments because of the substantial biases in model simulations of monsoons, which we also examine and which have persisted since the beginning of the CMIP exercise, as documented by [Lambert and Boer \(2001\)](#).

Although model biases have persisted since [Lambert and Boer \(2001\)](#), the representation of seasonal precipitation in

climate models has shown some improvement over the last two decades. Several studies reported slight improvements in climate models' representation of precipitation over monsoonal regions from CMIP phase 3 (CMIP3) to phase 5 (CMIP5) ([Monerie et al. 2012](#); [Brown et al. 2013](#); [Rienecker et al. 2012](#); [Joetzjer et al. 2013](#); [Sheffield et al. 2013](#); [Seo et al. 2013](#); [Sperber et al. 2013](#); [Grose et al. 2014](#); [Lee and Wang 2014](#); [Gulizia and Camilloni 2015](#); [Kusunoki and Arakawa 2015](#)). CMIP5 models showed slight improvements over CMIP3 models in simulating the observed climatological spatial and temporal precipitation patterns, the seasonal evolution of precipitation, precipitation extremes, the orientation of convergence zones, precipitation maxima in the vicinity of steep orography, and global monsoon domain and precipitation intensity ([Seo et al. 2013](#); [Sperber et al. 2013](#); [Lee and Wang 2014](#); [Gulizia and Camilloni 2015](#); [Kusunoki and Arakawa 2015](#)). CMIP5 models also showed improvements in the representation of the interannual variability of tropical precipitation ([Seo et al. 2013](#); [Joetzjer et al. 2013](#)), which is associated with improvements in the representation of El Niño–Southern Oscillation (ENSO) and teleconnection patterns (e.g., [Joetzjer et al. 2013](#)). Recent studies show that models participating in CMIP6 have improved representations of tropical precipitation over the ocean ([Tian and Dong 2020](#)), the Indian monsoon (e.g., [Gusain et al. 2020](#)), and the East Asian monsoon (e.g., [Xin et al. 2020](#)) in comparison to CMIP5 and CMIP3.

However, other aspects of precipitation associated with monsoons remain poorly represented in current climate models. Some examples are that the double ITCZ problem persists ([Li and Xie 2014](#); [Oueslati and Bellon 2015](#); [Zhang et al. 2015](#); [Tian and Dong 2020](#); [Fiedler et al. 2020](#)), the onset of the Indian

Corresponding author: Rodrigo J. Bombardi, rjbombardi@tamu.edu

monsoon is simulated too late (Sperber et al. 2013), summer monsoon precipitation over India and East Asia is underestimated (Sperber et al. 2013; Sooraj et al. 2015), precipitation over the Amazon basin is underestimated (Vera et al. 2006; Bombardi and Carvalho 2009; Yin et al. 2013; Gulizia and Camilloni 2015), and precipitation is underestimated along (sometimes incorrectly oriented) convergence zones such as the South Pacific convergence zone (SPCZ; Brown et al. 2013; Grose et al. 2014; Niznik et al. 2015), the South Atlantic convergence zone (SACZ; Vera et al. 2006), and the mei-yu–baiu front (Song and Zhou 2014).

In terms of projections for the end of the twenty-first century, some studies suggest that the global monsoon domain will expand (Hsu et al. 2013; Chen and Sun 2013; Lee and Wang 2014; Wang et al. 2020), although most of the expansion is expected to occur over the ocean (Lee and Wang 2014; Wang et al. 2020), with some expansion over land in Asia (Qing 2012; Lee and Wang 2014). A projected increase in precipitation over Asia is present in CMIP3 (e.g., Fan et al. 2012), CMIP5 (Qing 2012; Jiang and Tian 2013; Jourdain et al. 2013; Menon et al. 2013; Sharmila et al. 2015; Li et al. 2015), and CMIP6 (e.g., Ha et al. 2020; Wang et al. 2020) simulations. CMIP6 models project an increase in summer rainfall (Chen et al. 2020; He et al. 2020; Jin et al. 2020), wet season precipitation, wet season duration, and extreme precipitation over the Indian and East Asian monsoon regions (Ha et al. 2020; Moon and Ha 2020). CMIP5 models also project an increase in precipitation over Papua New Guinea in the twenty-first century (Jourdain et al. 2013). In contrast, there is no agreement between CMIP5 models regarding changes in monsoon rainfall over Indonesia and Malaysia (Jourdain et al. 2013). Narsey et al. (2020) also found no agreement between CMIP6 models regarding the magnitude or direction of changes in precipitation over northern Australia.

Global models have problems simulating the North American monsoon, with large errors in their representation of the mean annual cycle and the timing of the wet season (Geil et al. 2013; Sheffield et al. 2013). Future projections for the North American monsoon are inconsistent among models (Maloney et al. 2014). Geil et al. (2013) found that models tend to generate an unrealistic flux of low-level moisture from the tropics into the North American monsoon region, with a timing that unrealistically extends the monsoon season. Precipitation over the core South American monsoon region (the southern Amazon and central Brazil) is well represented by CMIP3 and CMIP5 models, including the seasonal cycle and interannual variability of precipitation (Vera et al. 2006; Vera and Silvestri 2009; Bombardi and Carvalho 2008, 2009; Jones and Carvalho 2013). Future projections indicate a southward shift of the SACZ, a delay in the onset of the South American monsoon (Seth et al. 2010, 2013), and a decrease in precipitation during the wet season over the core region of the South American monsoon (Bombardi and Carvalho 2009; Chen et al. 2020; He et al. 2020). Future projections also indicate an increase in precipitation over southern Brazil, Uruguay, and northern Argentina (Jones and Carvalho 2013; Chen et al. 2020).

Over Africa, future projections suggest a delay of the onset of the wet season over West Africa, an increase in precipitation

over the central-eastern Sahel, and a decrease in precipitation over the western Sahel (Monerie et al. 2012; Biasutti 2013; Roehrig et al. 2013; Chen et al. 2020). However, the lack of observational data in some regions makes it difficult to evaluate the models' representation of precipitation and their projections for future climate change, such as in the Congo region (Creese and Washington 2018). In addition, there are large differences in the models' representation of African monsoons and among the models' responses to climatic forcings (Biasutti 2013; Roehrig et al. 2013; Gaetani et al. 2017; Creese and Washington 2018; Chen et al. 2020).

Understanding future changes in monsoons, and thereby obtaining greater confidence in model projections, has been facilitated by various moist energy frameworks. Some of these employ the vertically integrated atmospheric moist static energy (MSE) budget, in which latent heating does not appear explicitly and large-scale flow can be seen as being forced by net energy fluxes through the top and bottom of the atmosphere (Neelin and Held 1987). Some vertically integrated energy budget frameworks can be used to causally relate changes in tropical circulations to high-latitude energy source anomalies, because the anomalous meridional energy flux needed to balance such high-latitude forcings is accomplished by quasi-diffusive eddy fluxes in the extratropics but by time-mean Hadley and monsoon flow in the tropics (e.g., Kang et al. 2008).

Other related frameworks do not leverage the MSE budget, but assume that precipitating convection acts on time scales that are fast compared to those of the large-scale flow of interest (e.g., seasonal monsoon circulations), yielding fluctuations of free-tropospheric temperature that are in quasi-equilibrium with fluctuations in near-surface MSE (Arakawa and Schubert 1974; Emanuel et al. 1994). Idealized models built on this convective quasi-equilibrium (CQE) assumption were used to show how zonal advection of extratropical dry air into monsoon regions limits the spatial extent of monsoon precipitation (Chou and Neelin 2001; Chou et al. 2001; Chou and Neelin 2003); this “ventilation” of the high-MSE tropical boundary layer by low-MSE extratropical air reduces the ability of the tropical region to convect. Related reasoning is employed in the “upped-ante” mechanism, in which the free-tropospheric temperature increases that occur in a warming world require larger near-surface MSE to achieve convective instability. When applied temporally to the seasonal cycle, this upped-ante mechanism was invoked to explain the delay in monsoon onset seen in some model simulations of future monsoons (Biasutti and Sobel 2009; Seth et al. 2011; Cook and Seager 2013). This delay in monsoon onset has also been referred to as an enhanced convective barrier, but it seems to only operate in simulations of some future monsoon regions (e.g., North America and West Africa) and not in others (e.g., South Asia), perhaps due to compensating increases in near-surface MSE (Seth et al. 2011). One of our goals here is to apply some of these ideas to the CMIP6 projections, and we find that changes in local near-surface MSE, perhaps caused by meridional energy fluxes, may be just as important as future enhancement or reduction of any convective barrier. We also

TABLE 1. Model description and references. Simulations with available near-surface temperature and humidity data for the calculation of near-surface moist static energy are indicated with an asterisk (*) for daily data and a hash mark (#) for monthly data.

Center/model	Resolution (lat × lon)	No. of ensemble members			Key references
		Historical	SSP370	SSP585	
Beijing Climate Center (BCC)/BCC-CSM2-MR	1.125° × 1.125°	3 (*, #)	1 (*, #)	1 (*, #)	Wu et al. (2019)
Canadian Centre for Climate Modeling and Analysis (CCCma)/CanESM5	2.8125° × 2.8125°	31 (*, #)	39 (*, #)	34 (*, #)	Swart et al. (2019)
Centre National de Recherches Météorologiques (CNRM)—Centre Européen de Recherche et de Formation Avancée en Calcul Scientifique (CERFACS)/CNRM-CM6-1	1.40625° × 1.40625°	13 (*, #)	1 (*, #)	1 (*, #)	Volodire (2018) , Volodire et al. (2019)
CNRM—CERFACS/CNRM-ESM2-1	1.40625° × 1.40625°	5 (*, #)	1 (*, #)	1 (*, #)	Séférian et al. (2016) , Séférian (2018)
Institute for Numerical Mathematics (INM)/INM-CM5-0	1.5° × 2.0°	1	1 (*, #)	—	Volodin et al. (2019)
Institut Pierre-Simon Laplace (IPSL)/IPSL-CM6A-LR	1.25° × 2.5°	32 (#)	4 (#)	—	Boucher et al. (2018)
Meteorological Research Institute (MRI)/MRI-ESM2-0	1.125° × 1.125°	5 (*, #)	1 (#)	—	Yukimoto et al. (2019)
National Center for Atmospheric Research (NCAR)/CESM2	0.9375° × 1.25°	10 (*, #)	1	2 (*, #)	Danabasoglu (2019a)
NCAR/CESM2-WACCM	0.9375° × 1.25°	3 (*, #)	1	—	Danabasoglu (2019b)
Geophysical Fluid Dynamics Laboratory (GFDL)/GFDL-CM4	1.0° × 1.25°	1 (*, #)	—	1 (*, #)	Guo et al. (2018)
GFDL/GFDL-ESM4	1.0° × 1.25°	1 (#)	1	1	Krasting et al. (2018)
Nanjing University Information Science and Technology (NUIST) Earth System Model version 3 (NESM3)/NUIST-NESM3	1.875° × 1.875°	1	—	1	Cao and Wang (2019)

present a new metric—the “relative MSE”—as a simple quantification of the lower- and upper-level influences on convective stability and an extension of the influential idea of “relative sea surface temperature” ([Vecchi and Soden 2007](#)).

This study is organized as follows. [Section 2](#) presents the data and methods used to characterize the rainy season over monsoonal regions. Analyses of seasonal precipitation for present and future climate are presented in [section 3](#). [Section 4](#) shows an examination of the characteristics of the wet season in historical and future scenario runs. [Section 5](#) provides some insights in the mechanism associated with changes in monsoon rainfall due to climate change. The main conclusions are presented in [section 6](#).

2. Data and methods

We used observed gridded precipitation data from the Global Precipitation Climatology Project (GPCP; pentads, global coverage at 2.5° spatial resolution, 1980–2016; [Xie et al. 2003](#); [Adler et al. 2003](#)), the Climate Hazards group Infrared Precipitation with Station data (CHIRPS; pentads, 50°S–50°N coverage at 0.05° spatial resolution, 1981–2016; [Funk et al. 2015](#)), and the Tropical Rainfall Measuring Mission (TRMM 3B42; 50°S–50°N coverage at 0.25° spatial resolution, 1998–2015; [Huffman et al. 2007](#)). In addition, we used 2-m temperature, 2-m dewpoint, and surface geopotential from the fifth generation of European Centre for Medium-Range Weather Forecasts (ECMWF) reanalysis (ERA5; daily, global coverage

at 0.75° horizontal spatial resolution, 1981–2010; [Hersbach et al. 2020](#)).

We also used daily precipitation, 2-m temperature, and 2-m specific humidity, and topography from 12 models participating in CMIP6. Three different scenarios were considered: historical runs and future scenarios represented by Shared Socioeconomic Pathways (SSPs) 3–7.0 (hereafter SSP3.70) and 5–8.5 (hereafter SSP5.85). The SSP5.85 scenario represents the upper range of forcings for future scenarios, corresponding to the CMIP5 RCP8.5 scenario. SSP3.70 represents a more moderate future forcing scenario ([Abram et al. 2019](#); [Kriegler et al. 2017](#); [Riahi et al. 2017](#)). [Table 1](#) shows details of models considered in this study.

We calculated the characteristics of the rainy and dry seasons (RADS; the characteristics are onset and demise dates, duration, and total precipitation during wet and dry seasons) at each grid point following the methodology described in [Bombardi et al. \(2019\)](#), which uses only precipitation data and is based on the methodology originally proposed by [Liebmann and Marengo \(2001\)](#). For each year, precipitation anomalies are created by simply subtracting the climatological annual mean precipitation from the precipitation at each time, yielding a time series of anomalies at each grid point. Starting from the date of the minimum in the first seasonal harmonic of the climatological mean annual cycle, which falls within the dry season for monsoon regions, we calculate cumulative precipitation anomalies in time. The cumulative precipitation anomaly for any given day is simply the sum of all precipitation anomalies from the start date

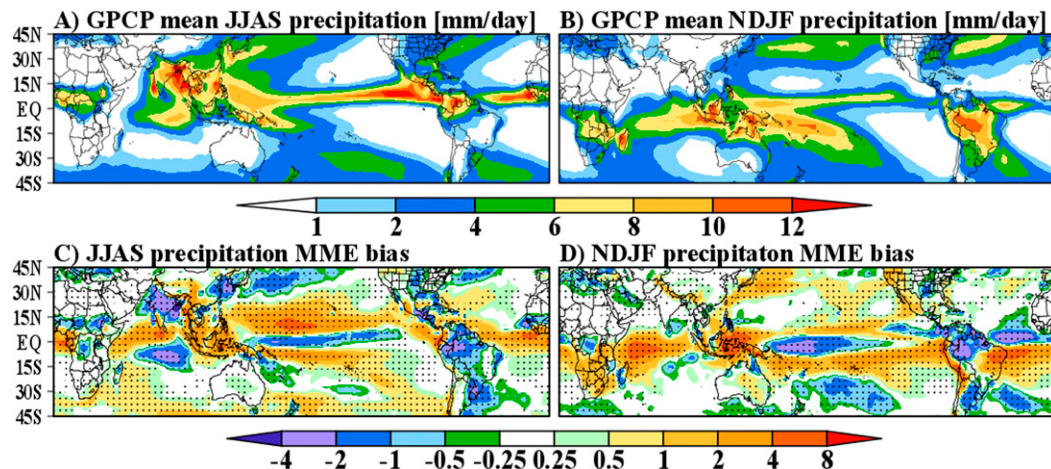


FIG. 1. Mean observed (GPCP) seasonal precipitation (mm day^{-1}) during (a) June–September and (b) November–February; MME bias of seasonal precipitation in historical runs during (c) June–September and (d) November–February. The period considered is from 1981 to 2010. The stippling represents grid points where at least 80% of the models have the same bias sign.

up to that same day. First, the onset of the rainy season is defined as the minimum value in the time series of cumulative precipitation anomalies. Then, a quality control test is applied to identify false onsets: for outliers, defined as years with onset dates outside 1.5 times the interquartile range, the onset is defined as the first date of the persistent change of sign of the first derivative of the smoothed time series of cumulative precipitation anomalies. Finally, the dataset is checked again for false onsets and any false onset is removed and flagged as missing data. The calculation of the demise date of the rainy season is calculated in the same way but backward (i.e., going back in time). Once the onset and demise dates are calculated, we calculate the duration of the dry and wet seasons and the accumulated precipitation during those seasons.

To calculate the characteristics of the rainy season for CMIP6 simulations we first calculated the climatological annual precipitation for each model from the historical experiment (from the ensemble mean for models with multiple realizations). Then, we calculated the characteristics of the rainy seasons for each realization (member) of each model (using their respective climatologies) in both the historical and scenario runs. Therefore, the parameters used to calculate the characteristics of the rainy season for scenario runs use the same climatological values used in the historical runs. We used the same climatological parameters for historical and scenario experiments to ensure the characteristics of the rainy season can be easily compared between experiments (i.e., we used the same baseline for each model). If multiple realizations are available for a single model, we first calculate statistics (e.g., mean, median, and interquartile range) for all realizations of that model before calculating multimodel ensemble (MME) statistics. Therefore, each model has the same weight in the MME statistics in any analyses reported here.

We also mask regions where the explained variance of the first harmonic of the mean annual cycle of precipitation is lower than that of the second or third harmonics. These regions

experience low seasonality or complex precipitation regimes (two or three rainy seasons per year). More details about the method can be found in Bombardi et al. (2019) and at the dataset website: <https://climatology.tamu.edu/research/Rainy-and-Dry-Season-RADS.html>. The advantage of masking these regions is that we remove from our analyses regions where the models have known deficiencies, such as poor representation of the annual cycle of precipitation or too wide ITCZs (e.g., Kim et al. 2008; Bombardi and Carvalho 2009). Therefore, we focus on regions with well-defined wet and dry seasons in observations and simulations.

3. Precipitation seasonal cycle

We first evaluate the models' errors and biases in representing seasonal precipitation over low-latitude regions. Figure 1 presents the observed (GPCP) mean precipitation for the extended boreal [June–September (JJAS)] and austral summer [November–February (NDJF)] and the MME bias and the MME root-mean-square error (RMSE). We use the number of models that have the same sign bias as an indication of agreement among models. The models overestimate precipitation over large parts of the tropical oceans, with exceptions over the eastern Indian Ocean, equatorial Pacific, and eastern North Atlantic, where precipitation is underestimated. These results indicate model deficiencies in representing convergence zones such as the mei-yu-baiu front (Fig. 1c), the SPCZ, and the SACZ (Fig. 1d). Many model deficiencies regarding tropical precipitation seem to be related to representation of the intensity, extent, and position of the ITCZ (Figs. 1c,d). The double ITCZ problem is still evident (Fig. 1d). Moreover, there is a remarkable agreement among models regarding the sign of precipitation biases, with more than 80% of models showing the same sign bias over most tropical and subtropical regions (Figs. 1c,d). The biases shown in Fig. 1 have been reported in CMIP3 and CMIP5 models (Vera et al. 2006; Kim et al. 2008;

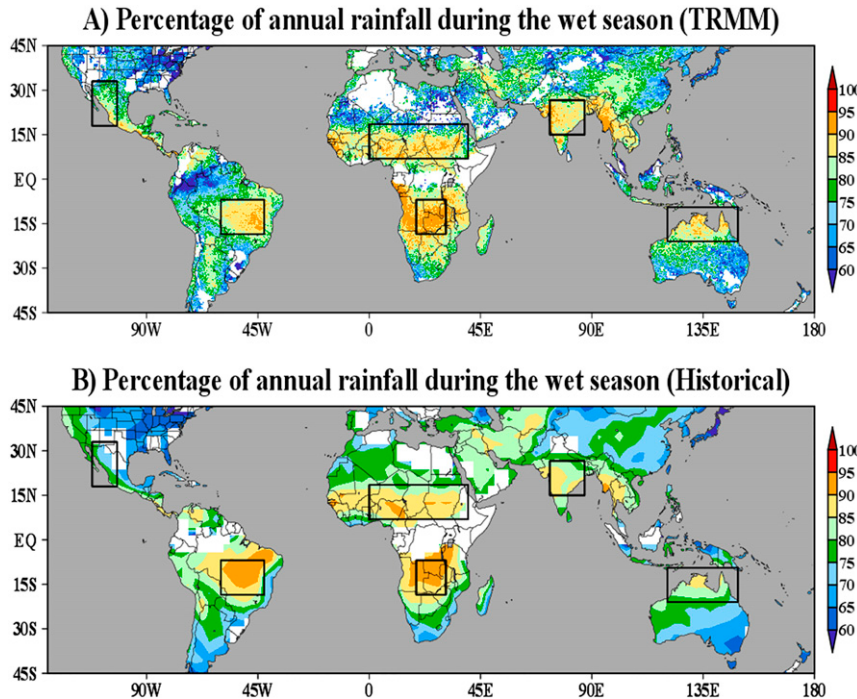


FIG. 2. Median percentage of annual precipitation that falls during the wet season for (a) precipitation from TRMM and (b) precipitation from historical runs (considering only models with available SSP370 simulations). The boxes in (a) indicate some of the regions of interest used for further analysis. Domains: North America (18° – 33° N, 248° – 258° E), South America (18.5° – 7° S, 300° – 318° E), Sahel (7° – 18.5° N, 0° – 40° E), southern Africa (18.5° – 7° S, 19.5° – 31° E), India (15° – 27° N, 73° – 87° E), and northern Australia (21° – 9.5° S, 120.5° – 149° E). Masked regions (in white) are regions with multiple wet season or regions without a clear wet season (see section 2 and Bombardi et al. 2019).

Bombardi and Carvalho 2009; Sperber et al. 2013; Yin et al. 2013; Grose et al. 2014; Song and Zhou 2014; Gulizia and Camilloni 2015; Sooraj et al. 2015) and in recent studies of CMIP6 (Tian and Dong 2020; Fiedler et al. 2020).

The global monsoon domain is commonly defined as the area where summer precipitation exceeds winter precipitation by a threshold of $2\text{--}2.5 \text{ mm day}^{-1}$ and summer precipitation exceeds 55% of annual precipitation (e.g., Hsu et al. 2013; Chen and Sun 2013; Lee and Wang 2014). However, this definition inherently includes transition areas between monsoonal and nonmonsoonal regimes. In this study we focus on core monsoonal regions, defined as regions where more than 80% of annual precipitation falls during the wet season (Fig. 2a). These regions include central South America [similar to domains used in Seth et al. (2010)], the Sahel region [similar to the domain used in Biasutti (2013) but focusing on the central Sahel], central southern Africa, India (commonly used domain for central India), and northern Australia [similar to the domain used in Narsey et al. (2020)]. Over subtropical monsoon regions such as North America [same domain used in Cook and Seager (2013)] the percentage of rain that falls during the wet season is lower in comparison to tropical monsoonal regions, but it still exceeds 70%. In most core monsoon regions, the models represent well the spatial pattern of the percentage of

annual precipitation that falls during the wet season. The largest biases are over subtropical regions such as western China and the North American monsoon region, in addition to northern Australia (Fig. 2b).

Figures 3 and 4 show the mean annual cycle of precipitation for observations and simulations over the regions of interest defined in Fig. 2. The models tend to simulate too much precipitation, compared to observations, during the whole year over the North American domain (Fig. 3a) with evident problems representing the onset and demise of the wet season. This is consistent with biases in CMIP3 and CMIP5 (e.g., Geil et al. 2013). Historical runs simulate the beginning of the wet season over the Sahel earlier than observed (Fig. 3b) and the beginning of the Indian monsoon later than observed (Fig. 3c), which is similar to CMIP5 simulations (Sooraj et al. 2015). The models also overestimate precipitation during the peak of the wet season over South America (Fig. 3d) and southern Africa (Fig. 3e), consistent with CMIP3 (Bombardi and Carvalho 2009). The mean annual cycle of precipitation over northern Australia shows a delay in historical runs relative to observations, where CHIRPS also show a negative bias in relation to GPCP and TRMM during the wet season (Fig. 3f). These results are consistent with the dry biases during local summer over the Sahel, India,

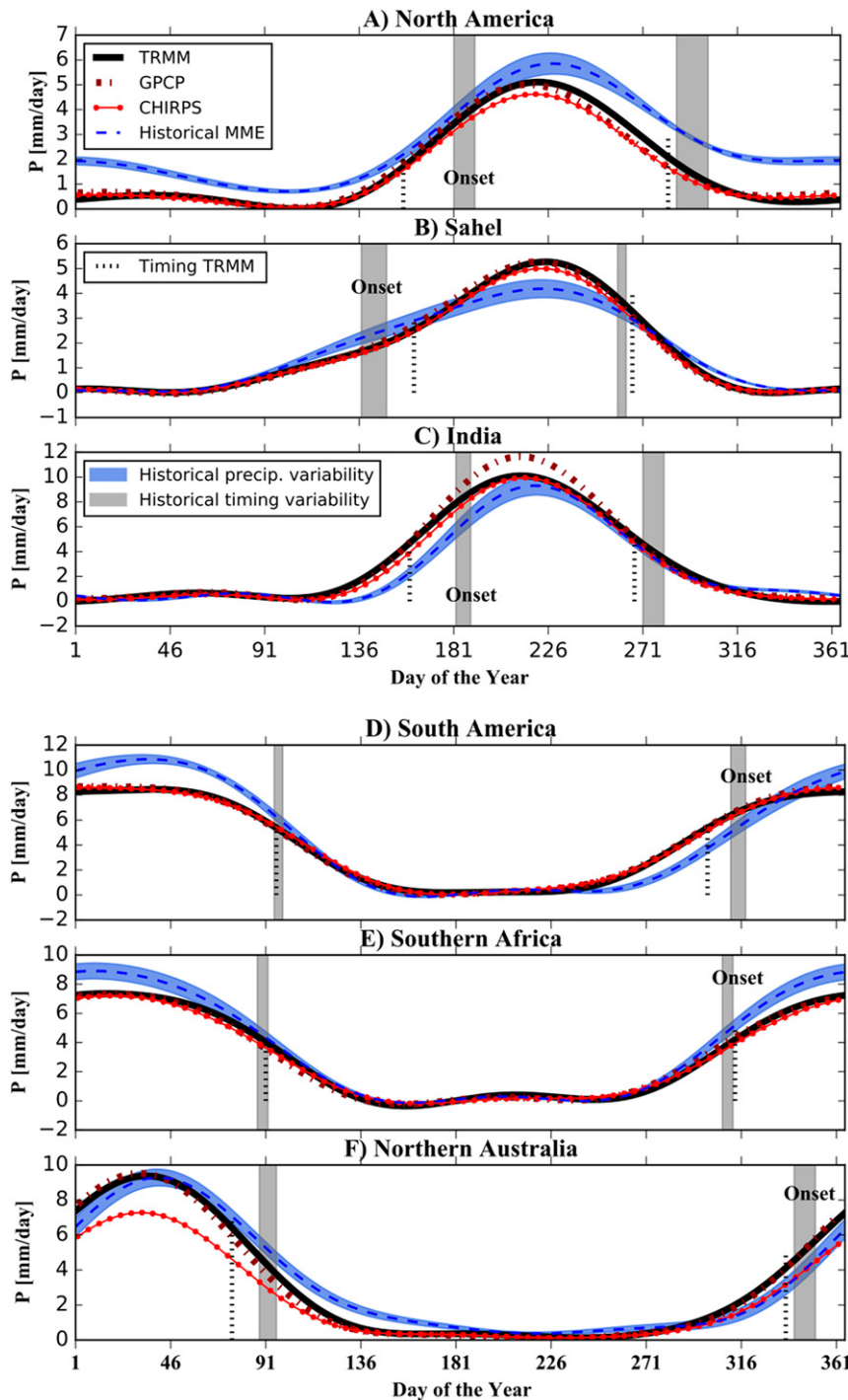


FIG. 3. Smoothed mean annual cycle of precipitation for observations and simulations spatially averaged over the regions shown in Fig. 2. Only values over land are included in the analysis. The figure includes the mean annual cycle of precipitation from GPCP, CHIRPS, and TRMM. For models with more than one integration, we first calculate the ensemble mean before calculating the MME mean to guarantee that each model has the same weight on the MME mean. The shading represents the MME spread as the standard error of the mean above and below the MME mean of historical runs. The vertical dashed line represents the median onset and demise dates for TRMM. The vertical shading indicates the MME mean of the median onset and demise dates of the full set of historical runs (12 models), plus and minus the standard error of the mean. The period considered is from 1981 to 2010. The mean annual cycle of precipitation in all datasets was smoothed using the first three harmonics.

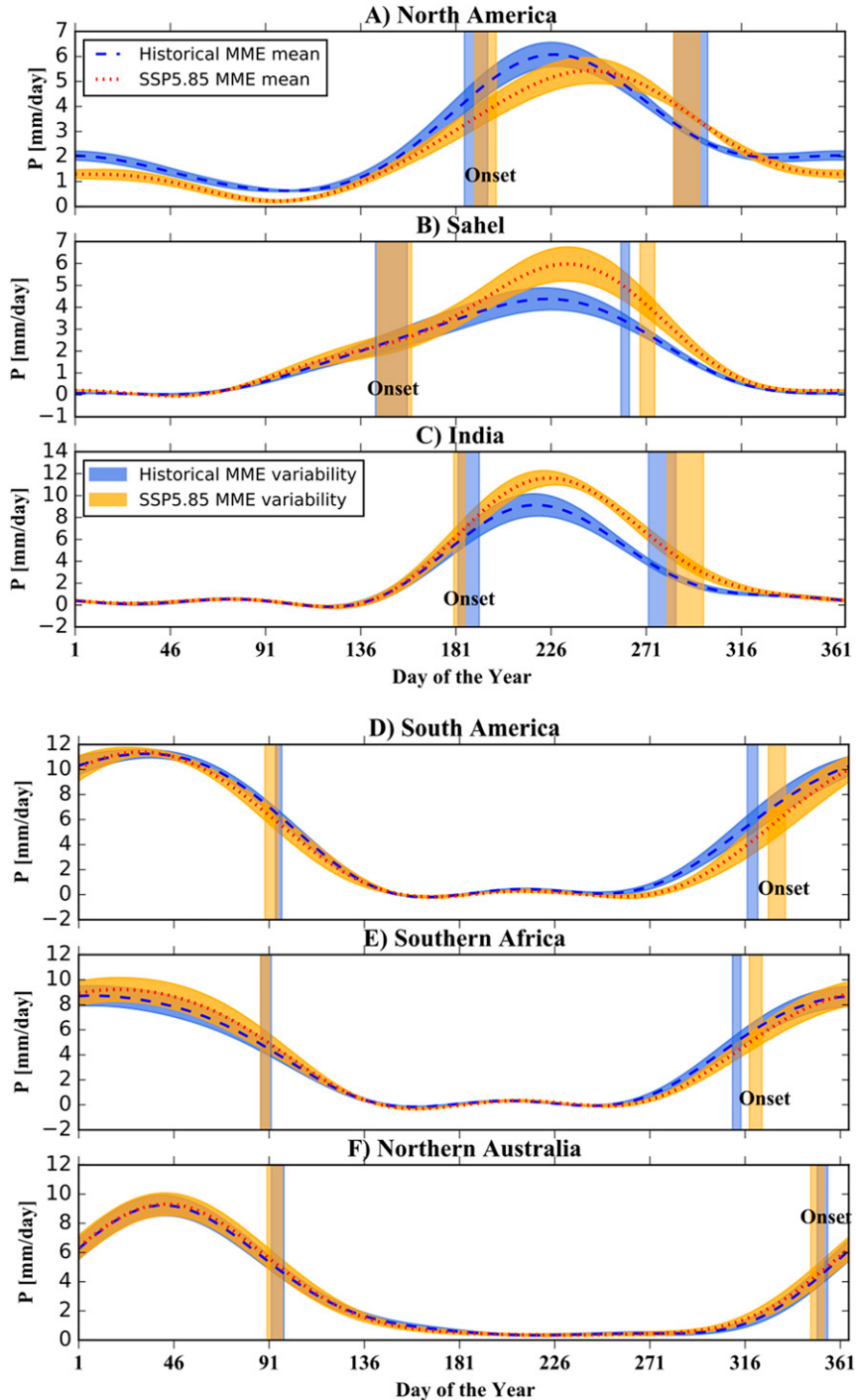


FIG. 4. Smoothed mean annual cycle of precipitation for historical and SSP5.85 simulations spatially averaged over the regions shown in Fig. 2. Only values over land are included in the analysis. Only models with available simulations for both scenarios were considered (eight models). The dashed line represents the MME mean of historical runs and the dotted line represents the MME mean of SSP5.85 runs. The shading represents the MME spread as one standard error of the mean above and below the MME mean. The vertical shading indicates the MME mean of the median onset and demise dates of the full set of historical runs (eight models), plus and minus the standard error of the mean. The period considered is from 1981 to 2010 for historical runs and from 2071 to 2100 for SSP5.85 runs. The mean annual cycle of precipitation was smoothed using the first three harmonics. Note that the shading has 70% opacity in order to allow comparison between experiments. The overlapping range between historical and SSP5.85 runs is denoted by the intermediate orange-blue hue.

and northern Australia (Figs. 1c,d) and wet biases over southern Africa and southeastern Brazil (Fig. 1d).

Turning to the future projections, SSP5.85 simulations suggest a decrease in peak monsoon rainfall and a temporal contraction of the rainy season over North America (Fig. 4a), and an increase in rainfall toward the end of the wet season with a delayed demise over the Sahel (Fig. 4b). Over India, SSP5.85 runs indicate an increase in peak monsoon rainfall as well as later demise dates (Fig. 4c). Over the remaining regions, SSP5.85 runs show smaller changes in the mean annual cycle of precipitation in comparison to historical runs (Figs. 4d–f), but with a later onset and earlier demise over both South America and southern Africa (Figs. 4e,f), and small changes to onset and demise over northern Australia (Fig. 4f). SSP3.70 runs show similar results (not shown).

4. Characteristics of the wet season in present and future climate simulations

In this section we analyze in more detail how well models simulate the characteristics of the rainy season (i.e., accumulated precipitation during the wet season and onset and demise dates) and their projections for future climate scenarios.

Figures 5 and 6 present boxplots showing interannual variability of the characteristics of the rainy season. These analyses used only one simulation from each model to avoid biasing the results toward models with multiple realizations. The boxplots were created by taking one value (the median over the core region) for each year for each dataset. For simulations, we take one value (the median) for each year for each model for each experiment. We also present boxplots of anomalous values of onset and demise dates calculated using median GPCP values as the reference, even for simulations.

If we compare the median values of observations and historical runs in Figs. 5 and 6, the results are consistent with the findings presented in Figs. 3 and 4. The simulations show a much larger range, due to the combination of intermodel scatter and interannual variability within each model (Figs. 5 and 6). It is worth mentioning that CHIRPS show very homogeneous values for demise dates over the Sahel (Fig. 5e), which suggests that the interannual variability of demise in that region is not well represented in CHIRPS. The range in historical and scenario simulations are often similar (Figs. 5 and 6) and the most evident differences are consistent with the results from Fig. 4. For example, scenario runs show a clear shift toward later demises over the Sahel (Fig. 5e) and later onsets over South America and southern Africa (Figs. 6a,d), associated with increased wet season rainfall in the Sahel (Fig. 5f) and lower wet season rainfall in South America and southern Africa (Figs. 6c,f). Scenario runs also show a shift toward a wetter Indian monsoon (Fig. 5i).

The differences between future scenario SSP5.85 and historical runs suggest a delay of the onset date over most of the Southern Hemisphere monsoon regions, in addition to tropical North America, far western Africa, and Southeast Asia under that climate change scenario (Fig. 7a). Earlier onset dates are simulated over the central and eastern Sahel and India. The future scenario suggests that the wet season will end later over

west Africa and the Sahel, much of Mexico, and parts of South and East Asia (Fig. 7b). Earlier demise dates are expected over most Southern Hemisphere monsoon regions. Consistent with the changes in wet season duration implied by these changes in onset and demise dates, the future scenario indicates an increase in wet season precipitation over most of the Northern Hemisphere monsoon zones, and a decrease over much of South America and southern Africa (Fig. 7c). These projections, which broadly correspond to an increase in wet season rainfall in the Northern Hemisphere and a decrease in the Southern Hemisphere, are consistent with projections from previous CMIP phases (Bombardi and Carvalho 2009; Seth et al. 2010; Fan et al. 2012; Qing 2012; Jiang and Tian 2013; Jourdain et al. 2013; Menon et al. 2013; Li et al. 2015; Sooraj et al. 2015; Monerie et al. 2012; Biasutti 2013; Roehrig et al. 2013), and more recent studies focusing on CMIP6 (e.g., Ha et al. 2020; Wang et al. 2021). Over northern Australia, there is little agreement among models regarding a change in wet season precipitation or a change in the timing of the wet season (Fig. 7), consistent with the findings of Narsey et al. (2020).

5. Possible energetic controls on rainfall trends

a. Motivating and defining the relative MSE

In this section we analyze surface air (2 m) MSE and its changes to better understand the mechanisms whereby climate change might affect monsoon rainfall. Most monsoon regions are sites of local maxima in surface air MSE (Fig. 8), with idealized theory predicting that monsoon rainfall should be concentrated on the equatorial side of these maxima (Nie et al. 2010). Surface air MSE is not a boundary condition or forcing for monsoons, but is set interactively by surface enthalpy fluxes, radiative cooling, and horizontal advection; nevertheless, its relationship with moist convective activity often allows the three-dimensional circulation and the precipitation field to be understood in terms of the two-dimensional MSE field [see review by Neelin (2007)].

As discussed in the introduction, it has been argued that monsoon onset will be delayed in a warming world if near-surface MSE in monsoon regions during early summer does not increase as rapidly as is needed to maintain convective instability given the free-tropospheric warming (Seth et al. 2011). In an attempt to quantify this effect, Seth et al. (2013) evaluated changes in atmospheric convective stability between historical and future scenario runs using the discretized vertical gradient of MSE (200-hPa MSE minus 850-hPa MSE). However, that vertical MSE gradient does not quantify known measures of convective stability. In particular, an atmospheric column is potentially unstable if its equivalent potential temperature (which is closely related to MSE) decreases upward, but this is a binary measure with a column being potentially stable or unstable; a quantitative measure is the convective available potential energy (CAPE), which can be approximated by differences of near-surface MSE and the saturation value of free-tropospheric MSE (e.g., Emanuel et al. 1994).

Thus, rather than use the Seth et al. (2013) metric, we note that the CQE frameworks on which the upped-ante idea is

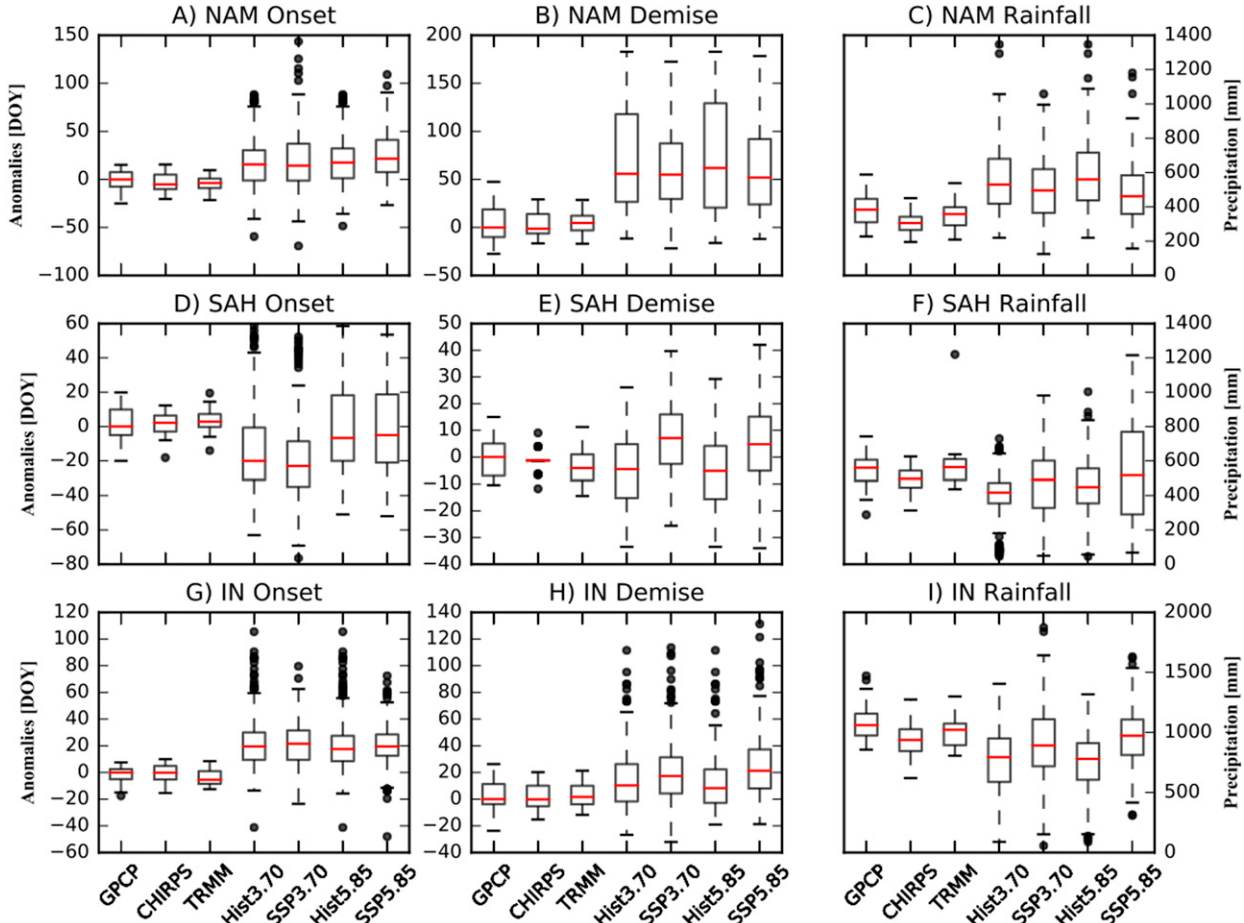


FIG. 5. Boxplot of the interannual variability of the characteristics of the rainy season. Horizontally, the frames show results for (a)–(c) the North American monsoon (NAM), (d)–(f) the Sahel (SAH), and (g)–(i) the Indian monsoon (IM) domains. Vertically, the frames show (left) onset, (middle) demise, and (right) wet season rainfall. Results are shown for three different precipitation observations as well as historical and scenario runs. Since there are different sets of models for scenario SSP3.70 and SSP5.85, the historical runs are showed twice, matching the models available in each future scenario. Thus, Hist3.70 represent historical runs for the same models in the SSP3.70 scenario. Likewise, Hist5.85 represent historical runs for the models in the SSP5.85 scenario. The analysis was carried out by first taking the median value for each year for each domain and then generating the boxplots. For this analysis, only one member from each model was included to avoid biases toward models with multiple realizations. Each model contributes one value (median over the domain) per year for each year of simulation during a 35-yr period. The box extends from the lower to upper quartile values of the data, with a line at the median. Whiskers are defined as 1.5 times the interquartile (75th–25th percentiles) range above or below the box. Fliers are points beyond the whiskers.

based (Chou and Neelin 2004) assume that tropospheric temperature in much of the tropics is set by near-surface MSE in convecting regions. Specifically, if near-surface MSE in a convecting region increases by Δh , gravity waves will spread any free-tropospheric warming throughout the tropics and thus require that all remote regions undergo an increase of Δh in their near-surface MSE in order to maintain a constant degree of convective instability. Such relationships have been shown to couple near-surface MSE over land and ocean in observations (Zhang and Fueglistaler 2020). This motivates us to define the “relative MSE” as the local near-surface MSE minus the tropical mean (20°S – 20°N ; all longitudes, land and ocean) near-surface MSE. This is a generalization of “relative sea surface temperature” (SST), which has been influential in

understanding variations in tropical cyclone activity (Vecchi and Soden 2007; Swanson 2008; Ramsay and Sobel 2011), with an important aspect of this generalization being that it is defined in land regions (unlike relative SST). A possible benefit of both relative MSE and relative SST is that they capture the local and large-scale forcings for convection, rather than relying on local, column-wise measures such as CAPE or the local vertical gradient of MSE (Seth et al. 2013) that are expected to be rapidly adjusted by convective activity.

In every monsoon region, surface air MSE reaches its peak in summer, between the local onset and demise dates (Fig. 9). In each region, the MSE has roughly the same value on the onset date as on the demise date; since these dates are defined using only precipitation, this lends confidence in the

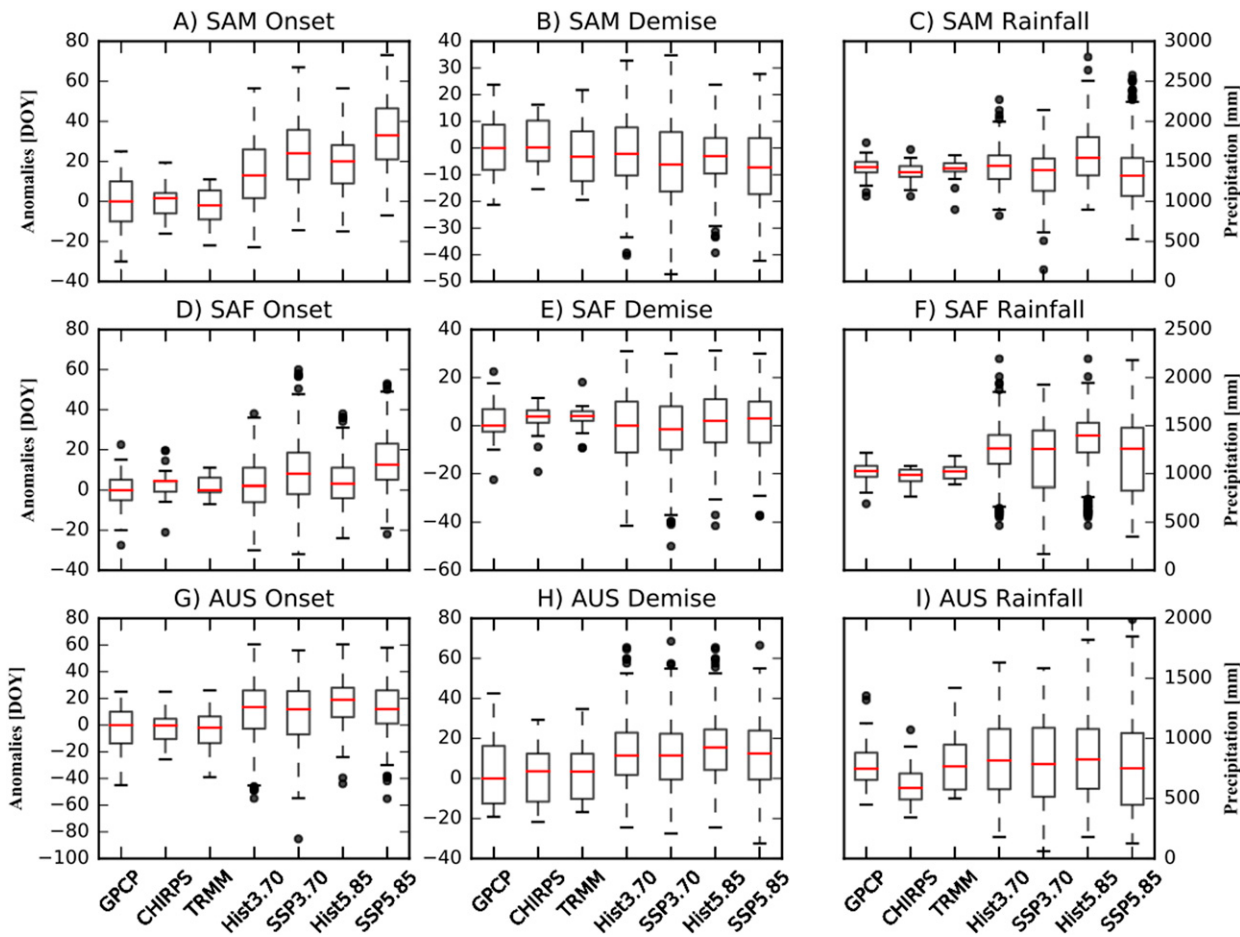


FIG. 6. As in Fig. 5, but for (a)–(c) the South American monsoon (SAM), (d)–(f) southern Africa (SAF), and (g)–(i) northern Australian monsoon (AUM) regions.

connection of MSE to precipitation and the timing of the rainy season. Additionally, some of the most prominent CMIP6 biases in monsoons are consistent with the MSE biases: large negative MSE biases over India and South America from winter through early summer accompany the late onset biases in those regions (Figs. 9c,d). There is variability across regions in the MSE values at which onset and demise occur, ranging from about 340 kJ kg^{-1} in North America and the Sahel to 350 kJ kg^{-1} in India; since the tropical mean surface air MSE is around 339 kJ kg^{-1} , with relatively little seasonal and interannual variation (not shown), onset and demise occur at different relative MSE values in each region. This is not surprising, given the many assumptions and simplifications involved in relating large-scale precipitating circulations to surface air MSE. So we hypothesize that the rainy season begins when the relative MSE first increases beyond some threshold, with this threshold varying between regions due to differences in factors that might affect the relation of relative MSE to precipitation, such as free-tropospheric dry air intrusions (Parker et al. 2016) and the vertical structure of ascent (Back and Bretherton 2006). We furthermore hypothesize that this relative MSE threshold will remain

invariant under climate change within each region; this is examined further below.

b. Future changes in relative MSE

As expected in a warming world, the models indicate an increase in mean near-surface MSE for all days of the year under scenarios SSP3.70 and SSP5.85, compared to historical runs. The mean annual cycle of relative MSE in monsoon regions has similar temporal structure for historical and future scenario simulations, reaching minimum values during local winter and maximum values during summer (Fig. 9). Figure 10 shows the mean annual cycle of the change in relative MSE between scenario (SSP5.85) and historical runs; positive values occur when a region's near-surface MSE increases more than that of the rest of the tropics, indicating an expected future increase in convective instability. Over all core monsoonal regions, relative MSE differences are generally positive during the wet season and negative during the dry season. This is consistent with findings of Giannini (2010) and Seth et al. (2013), who argued that models show a dominance of free-tropospheric warming and thus greater convective stability in winter, while near-surface warming and moistening and thus

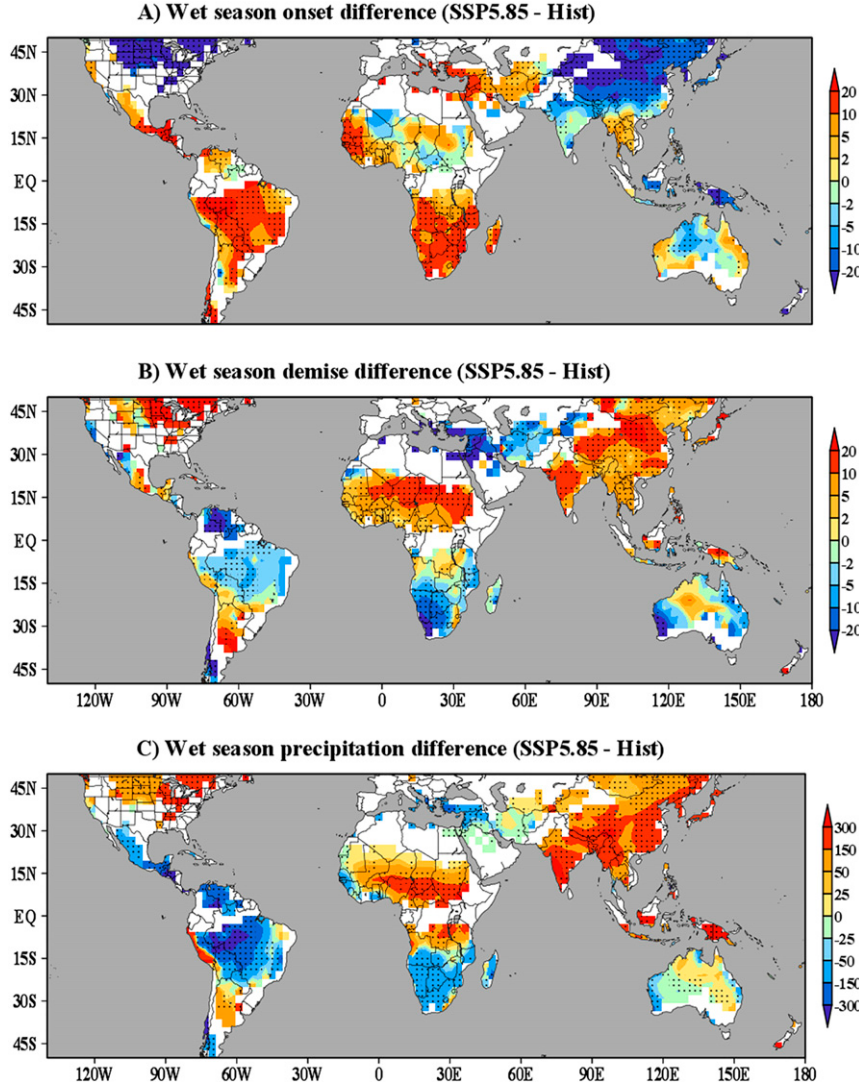


FIG. 7. Difference between future scenario SSP5.85 and historical runs for (a) median onset date, (b) median demise date, and (c) median total precipitation during the wet season. Stippling indicates regions where at least 7 out of 10 models show the same difference sign. Masked regions (in white) are regions with multiple wet season or regions without a clear wet season (see section 2; see also [Bombardi et al. 2019](#)).

greater instability dominated in summer. Of course, true convective stability involves the full vertical structure of temperature and humidity, especially when one accounts for possible entrainment of environmental air into clouds (e.g., [Emanuel et al. 1994](#); [Derbyshire et al. 2004](#)), so these changes in relative MSE are crude and incomplete indicators of the combined local and remote forcings for convective activity; we do not claim that a mean summer increase in relative MSE signifies a larger mean summer convective mass flux.

The more salient features seen in [Fig. 10](#) are the future changes in relative MSE occurring around onset and demise dates. Most prominent are the increases in relative MSE before monsoon onset and after demise in India ([Fig. 10c](#)), which are accompanied by the earlier onset and later demise expected in

our relative MSE framework. The Sahel also shows a large increase in relative MSE in late summer, together with a future delay in its demise date ([Fig. 10b](#)). Both South America and southern Africa show reductions in relative MSE near the historical onset date, and the corresponding expected delay in future onset ([Figs. 10d,e](#)).

Other changes in relative MSE near onset and demise dates are smaller, at least in the multimodel mean shown in [Fig. 10](#), which motivates inspection of the intermodel variations in changes in both relative MSE and onset/demise dates. There is a strong correlation between future changes in relative MSE in a region and future changes in its onset/demise dates ([Fig. 11](#)). As expected by the logic used to motivate our construction of the relative MSE diagnostic, models with larger

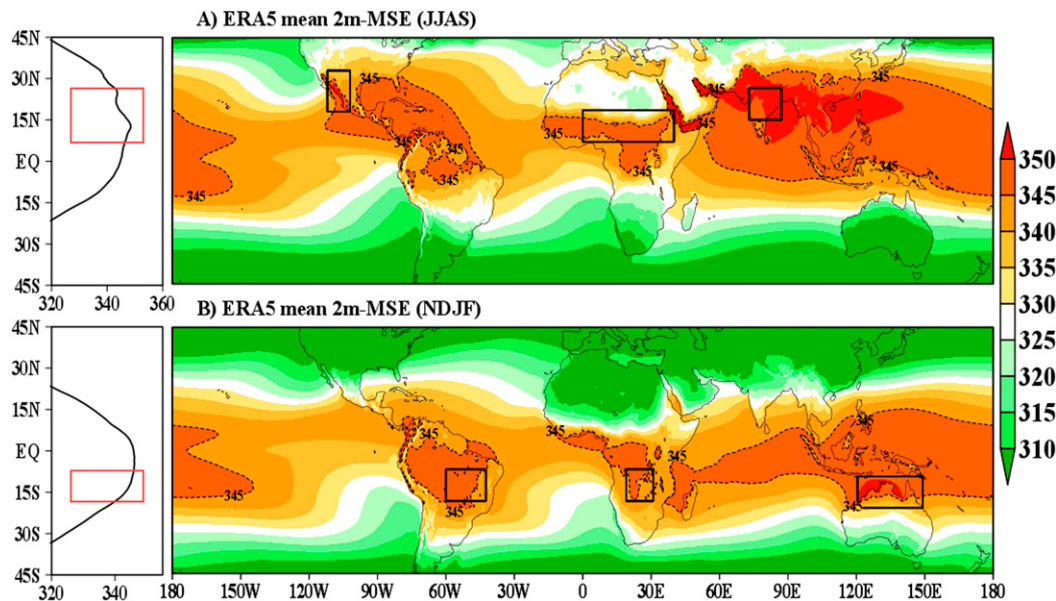


FIG. 8. Seasonal spatial pattern and zonal mean of observed (ERA5) near-surface MSE (kJ kg^{-1}) during (a) June through September and (b) November through February. Dashed contours show the value of 345 kJ kg^{-1} , highlighting that the maximum near-surface MSE values occur over monsoonal regions. The boxes show the monsoon domains of interest. In (a), the box in the zonal mean frame comprises the domain of both India and Sahel. In (b), the box in the zonal mean frame comprises the domains of both South America and southern Africa. The period considered is from 1981 to 2010.

future increases in relative MSE in early summer exhibit earlier onset, and models with larger future increases in relative MSE in late summer exhibit later demise. The intermodel variability in the relative MSE changes explains 50%–80% of the intermodel variance in onset and demise dates, and the coefficients of the best linear fit to intermodel variability for the SSP3.70 scenario are nearly the same as those for the SSP5.85 scenario. The linear fits indicate that, for no change in relative MSE, there is a delay in onset and an earlier demise by roughly five days; in other words, to maintain the same onset date an increase in relative MSE is required. We do not investigate here whether this results from error in the fit, an expected relationship between relative MSE and convective onset in a warming world, a peculiarity of model convection schemes, a result of changes in tropical-mean near-surface MSE in regions that are convectively stable, or some other factor.

c. Meridional gradients in MSE

Although changes in relative MSE are strongly correlated with changes in onset and demise dates (Fig. 11), the former cannot be viewed as causing the latter because MSE can be rapidly altered by horizontal advection, radiation, and surface fluxes. Some constraint on the large-scale processes that influence monsoon-region MSE or tropical-mean MSE would be better viewed as a cause, and here we draw attention to changes in the tropical–extratropical contrast in MSE in the model projections. This contrast is central to vertically integrated energy budget frameworks that link changes in

monsoon precipitation to changes in meridional energy fluxes (Kang et al. 2008; Schneider et al. 2014; Boos and Korty 2016), which in turn scale with the magnitude of the meridional gradient in surface air MSE under a diffusive approximation (Hwang and Frierson 2010; Merlis and Henry 2018; Peterson and Boos 2020).

Figure 12 presents spatial distributions of relative MSE changes during the onset and demise periods for four core monsoon regions. Relative MSE changes are averaged over all models and over the month when each model's median onset (or demise) date occurs in historical runs, with this procedure performed for each core monsoon region. The spatial patterns of relative MSE changes are similar for monsoons from the same hemisphere (not shown), so results for India are shown in Figs. 12a and 12c and results for South America in Figs. 12b and 12d. The figure also includes zonal means of the relative MSE change for those two regions (solid lines in left panels) as well as zonal means for the months of onset and demise over the Sahel and southern Africa (dashed lines in left panels).

The most prominent pattern is the large meridional gradient in the change of relative MSE, which has greatest magnitude in the Southern Hemisphere. That is, in the Southern Hemisphere of a warming world, monsoon regions undergo onset and demise in a hemispheric background state possessing an enhanced tropical–extratropical MSE gradient. One would expect this enhanced meridional MSE gradient to facilitate greater advection of low-MSE air into the Southern Hemisphere monsoon regions, or equivalently a vertically integrated flux of MSE out of those regions (e.g., Hwang and Frierson 2010),

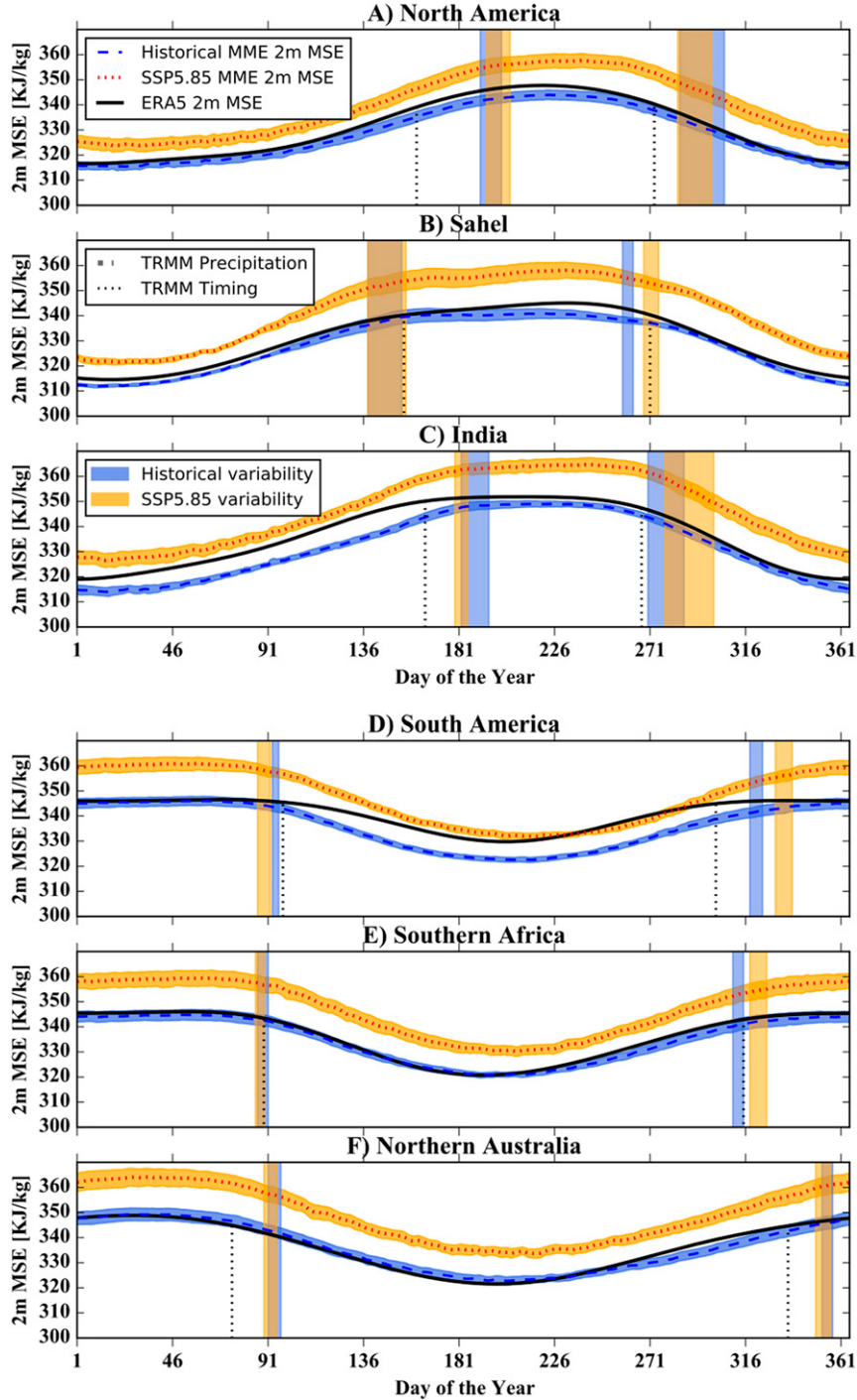


FIG. 9. Smoothed mean annual cycle of near-surface MSE for observations (thick solid black line, ERA5) as well as historical and SSP5.85 simulations, spatially averaged over the regions shown in Fig. 2. Only values over land are included in the analysis. Only models with available simulations for both scenarios were considered (eight models). The shading represents the MME spread as one standard error of the mean above and below the MME mean. The vertical shading indicates the MME mean of the median onset and demise dates of the full set of historical runs (eight models), plus and minus the standard error of the mean. The vertical dashed line shows the median onset and demise dates from TRMM. The thick dashed line shows the observed mean annual cycle of precipitation from TRMM. The period considered is from 1981 to 2010 for observations and historical runs and from 2071 to 2100 for SSP5.85 runs. The mean annual cycle was smoothed using the first three harmonics. Note that the shading has 70% opacity in order to allow comparison between experiments. The overlapping range between historical and SSP5.85 runs is denoted by the intermediate orange–blue hue.

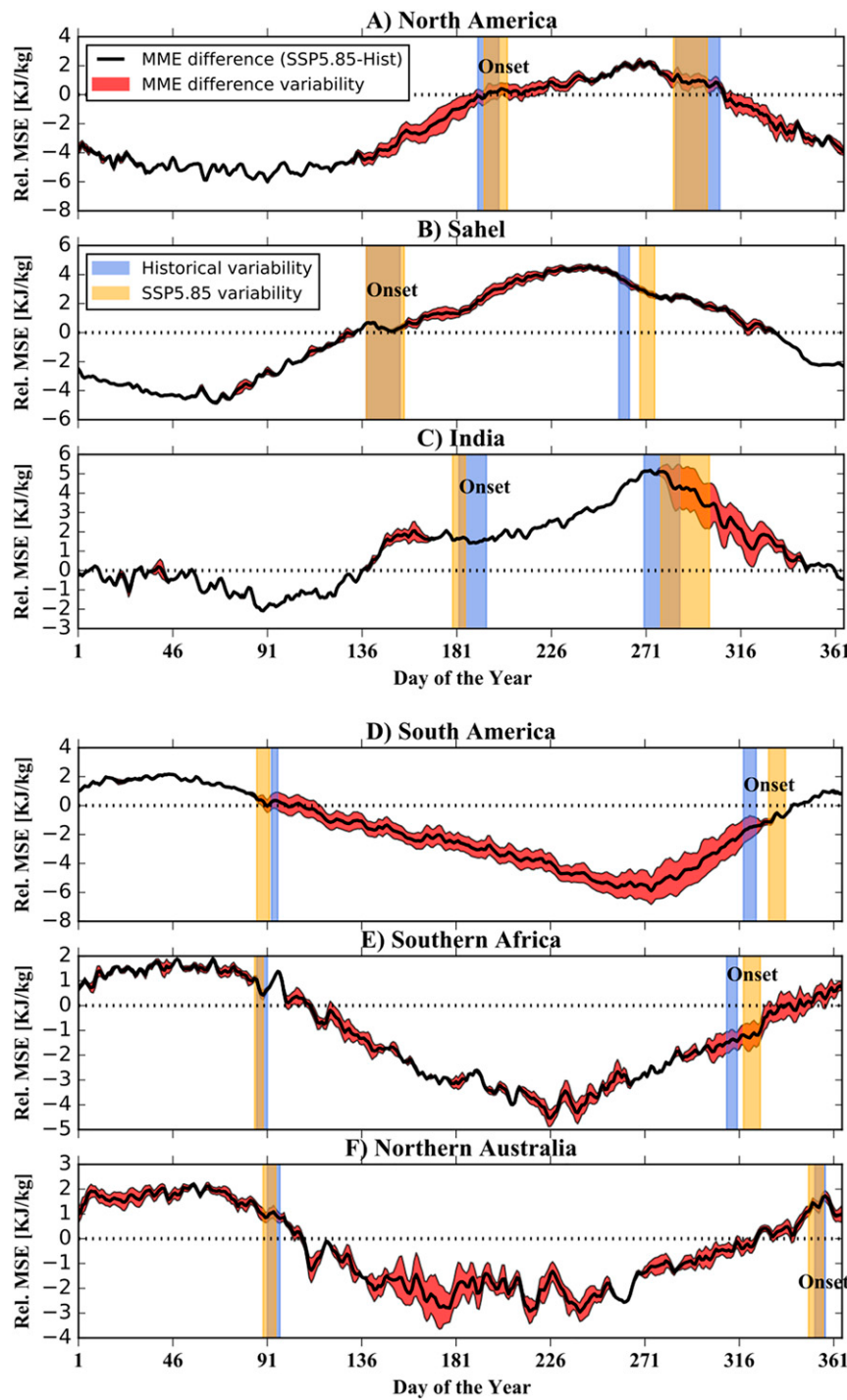


FIG. 10. Difference between SSP5.85 and historical mean annual cycle of relative surface MSE. Values are spatially averaged over the regions shown in Fig. 2. Only values over land are included in the analysis. Only models with available simulations for both scenarios were considered (six models). For models with more than one integration, we first calculate the ensemble mean before calculating the MME mean to guarantee that each model has the same weight on the MME. The shading represents the spread in simulations as one standard error of the mean above and below the MME mean. The period considered for historical runs is from 1981 to 2010 and the period considered for SSP5.85 runs is from 2071 to 2100. Vertical shadings show the MME variability (mean plus and minus one standard error of the mean across all models) for onset and demise dates for each experiment.

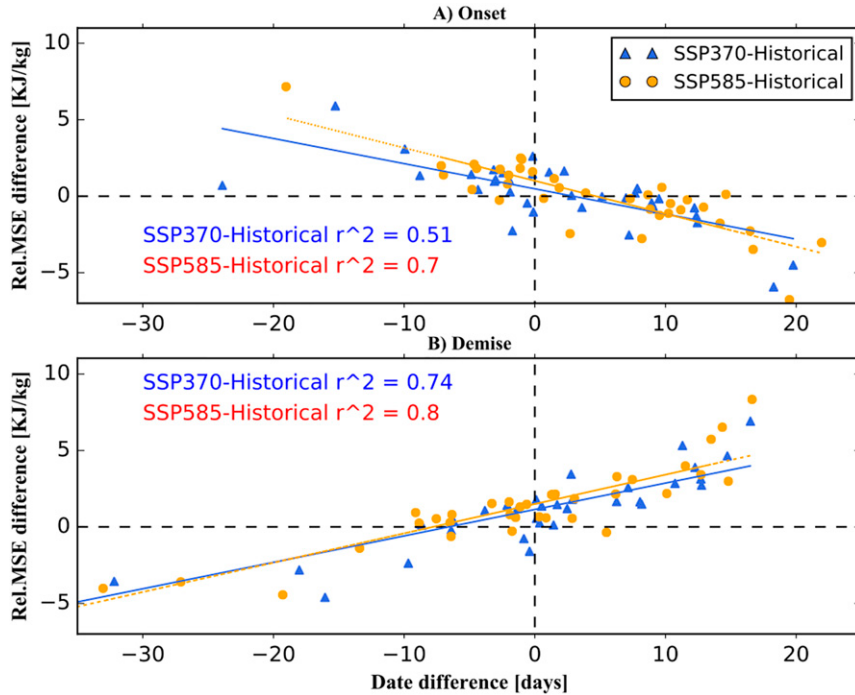


FIG. 11. Scatterplot of the difference (scenario minus historical runs) in relative near-surface MSE as a function of (a) onset date difference and (b) demise date differences. The plots include values from all core monsoon regions (Fig. 2). Each value of onset, demise, or relative near-surface MSE is calculated as the spatial average over each core monsoon region. Relative near-surface MSE averages are taken over the period the mean onset (or demise) month for each member of each model. The figure also includes the best linear fit for each scenario. All r^2 are statistically significant at 5% level.

decreasing the local monsoon-region MSE and reducing rainfall. Indeed, rainy season onset is delayed in projections of most of the Southern Hemisphere regions (Fig. 12b), demise occurs earlier (Fig. 12d), and wet season precipitation is reduced (Fig. 7c). Northern Australia is a partial exception to this pattern, with less agreement between models there. The Northern Hemisphere monsoon regions undergo onset in a global background state with relatively little change in that hemisphere's tropical-extratropical MSE gradient (Fig. 12a), and the Northern Hemisphere exhibits a general dominance of earlier onset (Fig. 12a), later demise (Fig. 12c), and more wet season precipitation (not shown, but similar to Fig. 7c). We speculate that a general increase in amplitude of the seasonal cycle of rainfall would occur in a warming world with no change in meridional MSE gradient due to greater moisture content (e.g., Held and Soden 2006), leading to earlier onset, later demise, and more wet season rainfall; this overall enhancement of rainfall would then be the background change that is opposed in the Southern Hemisphere by the enhanced tropical-extratropical MSE gradient.

6. Conclusions

We evaluated the representation of the characteristics of the wet season over core monsoonal regions by a subset of simulations performed as part of the new WCRP-CMIP6. We also

investigated future projections of the characteristics of the wet season in a subset of CMIP6 models. Our analysis included evaluation of the seasonal cycle of precipitation, the timing of the wet season, and the accumulated precipitation during the wet season. We also investigated the role of atmospheric stability, as measured by relative MSE, in changing the precipitation seasonal cycle.

The characteristics of the wet season (onset, demise, and accumulated precipitation) were calculated using a consistent method across monsoonal regions based on the RADS methodology by Bombardi et al. (2019). We find that, in general, the summer monsoon in the central Sahel and Asia is projected to withdraw later and become wetter in comparison to historical runs. In contrast, the summer monsoon over South America and southern Africa are projected to start later and become drier in comparison to historical runs.

The models still have serious deficiencies in representing tropical precipitation. Among some of the most concerning problems are the following:

- poor representations of the seasonal cycle of precipitation over the North American monsoon domain, especially during the withdrawal of the wet season;
- poor representation of the onset of the Indian monsoon and an overall dry bias over the Indian and East Asian monsoon domains; and

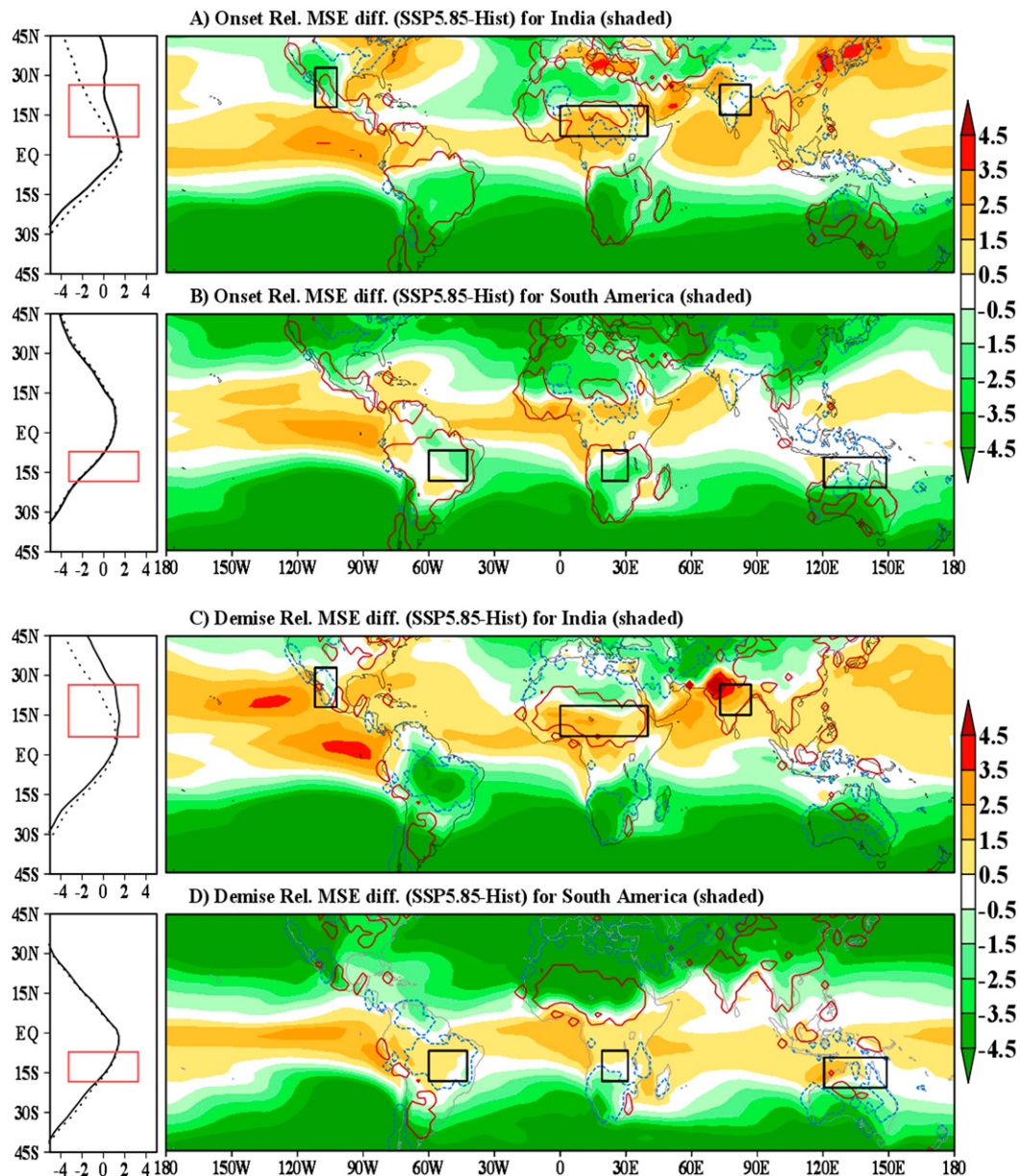


FIG. 12. Spatial pattern and zonal mean of MME average of relative near-surface MSE differences (SSP5.85 – Historical) during the *onset* over (a) India (shading and zonal mean solid line) and the Sahel (zonal mean dashed line) and (b) South America (shading and zonal mean solid line) and southern Africa (zonal mean dashed line). (c),(d) As in (a) and (b), but during the *demise*. Averages are calculated for the median onset (or demise) month in the historical run of each model. Solid red contours indicate positive changes of 3 days in onset dates in (a) and (b) and demise dates in (c) and (d). Dashed blue contours indicate negative changes of 3 days in onset dates in (a) and (b) and demise dates in (c) and (d). Zonal means are calculated over the whole tropics. Only models with available simulations for both scenarios were considered (six models).

- dry bias over the Amazon region and wet bias over northeast Brazil, and, to a lesser extent, dry biases over the Sahel.

Although accurate simulation of present-day climate does not guarantee reliable projection of the future, it seems worthwhile to clearly state the projections for regions that do

have low bias in their historical simulations. These include the following:

- There will very likely be shortening of the wet season over South America (later onset and early demises), associated with a decrease in total rainfall during the rainy season.

- There will likely be shortening of the wet season over southern Africa (late onsets) associated with a decrease in mean total rainfall during the rainy season over southern Africa.
- An extension of the wet season over India (later demises) will occur associated with an increase in wet season rainfall, which is consistent with previous studies (e.g., Wang et al. 2020, 2021). However, uncertainties in the representation of the onset date of the Indian monsoon suggest that these projections should be interpreted with caution since the model simulations of early summer rainfall are strongly biased.
- There is substantial spatial variability in the characteristics of the rainy season over West Africa and the Sahel. Therefore, changes in wet season characteristics across the Sahel due to climate change may vary from region to region. For example, projections show different results for coastal West Africa and the continental Sahel. Over the core region we selected to study, the models project an extension of the wet season (later demises) associated with an increase in wet season precipitation. However, uncertainties in observations and simulations suggest that these projections should be interpreted with caution.
- There is no agreement in models' projections for the timing of the wet season or in the accumulated precipitation during the wet season over northern Australia, consistent with Narsey et al. (2020).

Future projections of changes in the timing of monsoons are well captured by changes in near-surface relative MSE. Simulations indicate that the Sahel and India will experience longer wet seasons associated with near-surface MSE increasing in those regions by more than the tropical mean during the historical onset and demise periods. The opposite is expected for South America and southern Africa, which have decreases in relative MSE during the historical onset periods. In the Southern Hemisphere, where those two regions lie, the tropical-extratropical gradient in MSE is projected to increase, which we speculate might lead to more cold and dry extratropical air penetrating into those regions (or, equivalently, more quasi-diffusive transport of MSE out of those regions). Although meridional fluxes of MSE between monsoon regions and higher latitudes have been shown to cause rainfall changes in monsoon regions (e.g., Kang et al. 2008; Boos and Korty 2016; Peterson and Boos 2020), further work is needed to determine whether the Southern Hemisphere's enhanced meridional MSE gradient in future projections truly causes the shortening of that hemisphere's summer monsoons.

The dry biases over India, eastern Asia, and the Amazon are deficiencies that have been present in climate models since CMIP3. In addition, the models still show large deficiencies in representing precipitation in convergence zones (such as the mei-yu-baiu front, SPCZ, and SACZ) associated with monsoon systems. Without a better representation of these features, confidence in future projections of climate change over regions affected by these features (i.e., southeastern Brazil and eastern China) is compromised.

Although many of the analyses presented in this study show results for all regions within 45° of the equator, these analyses are most reliable over monsoonal regions. While some regions

in midlatitudes, such as the Great Plains in the United States, experience moderate precipitation seasonality, the definitions of onset and demise dates over these regions are less accurate than over monsoonal regions (Bombardi et al. 2019). Therefore, projections of future changes in onset and demise dates and wet season precipitation over these regions should be interpreted with caution.

Acknowledgments. We acknowledge the World Climate Research Programme, which, through its Working Group on Coupled Modelling, coordinated and promoted CMIP6. We thank the climate modeling groups for producing and making available their model output, the Earth System Grid Federation (ESGF) for archiving the data and providing access, and the multiple funding agencies who support CMIP6 and ESGF. This material is based upon work supported by the U.S. Department of Energy, Office of Science, Office of Biological and Environmental Research, Climate and Environmental Sciences Division, Regional and Global Model Analysis Program, under Award DE-SC0019367. It used resources of the National Energy Research Scientific Computing Center (NERSC), which is a DOE Office of Science User Facility. We thank DOE's RGMA program area, the Data Management program, and NERSC for making this coordinated CMIP6 analysis activity possible. We thank Drs. Jim Kinter, Kathy Pegion, Phil Pegion, and the three anonymous reviewers for their helpful comments to improve this paper.

REFERENCES

- Abram, N., and Coauthors, 2019: Framing and context of the report supplementary material. *IPCC Special Report on the Ocean and Cryosphere in a Changing Climate*, IPCC, 1–11.
- Adler, R. F., and Coauthors, 2003: The version-2 Global Precipitation Climatology Project (GPCP) monthly precipitation analysis (1979–present). *J. Hydrometeor.*, **4**, 1147–1167, [https://doi.org/10.1175/1525-7541\(2003\)004<1147:TVGCP>2.0.CO;2](https://doi.org/10.1175/1525-7541(2003)004<1147:TVGCP>2.0.CO;2).
- Arakawa, A., and W. H. Schubert, 1974: Interaction of a cumulus cloud ensemble with the large-scale environment, Part I. *J. Atmos. Sci.*, **31**, 674–701, [https://doi.org/10.1175/1520-0469\(1974\)031<0674:IOACCE>2.0.CO;2](https://doi.org/10.1175/1520-0469(1974)031<0674:IOACCE>2.0.CO;2).
- Back, L. E., and C. S. Bretherton, 2006: Geographic variability in the export of moist static energy and vertical motion profiles in the tropical Pacific. *Geophys. Res. Lett.*, **33**, L17810, <https://doi.org/10.1029/2006GL026672>.
- Biasutti, M., 2013: Forced Sahel rainfall trends in the CMIP5 archive. *J. Geophys. Res. Atmos.*, **118**, 1613–1623, <https://doi.org/10.1002/jgrd.50206>.
- , and A. H. Sobel, 2009: Delayed Sahel rainfall and global seasonal cycle in a warmer climate. *Geophys. Res. Lett.*, **36**, L23707, <https://doi.org/10.1029/2009GL041303>.
- Bombardi, R. J., and L. M. V. Carvalho, 2008: Variability of the monsoon regime over the Brazilian savanna: The present climate and projections for a 2xCO₂ scenario using the MIROC model. *Rev. Bras. Meteor.*, **23**, 58–72, <https://doi.org/10.1590/S0102-77862008000100007>.
- , and —, 2009: IPCC global coupled model simulations of the South America monsoon system. *Climate Dyn.*, **33**, 893–916, <https://doi.org/10.1007/s00382-008-0488-1>.
- , J. L. Kinter, and O. W. Frauenfeld, 2019: A global gridded dataset of the characteristics of the rainy and dry seasons. *Bull.*

- Amer. Meteor. Soc.*, **100**, 1315–1328, <https://doi.org/10.1175/BAMS-D-18-0177.1>.
- Boos, W. R., and R. L. Korty, 2016: Regional energy budget control of the intertropical convergence zone and application to mid-Holocene rainfall. *Nat. Geosci.*, **9**, 892–897, <https://doi.org/10.1038/ngeo2833>.
- Boucher, O., S. Denvil, A. Caubel, and M. A. Foujols, 2018: IPSL IPSL-CM6A-LR model output prepared for CMIP6 CMIP. Earth System Grid Federation, accessed June 2020, <https://doi.org/10.22033/ESGF/CMIP6.1534>.
- Brown, J. N., and Coauthors, 2013: Implications of CMIP3 model biases and uncertainties for climate projections in the western tropical Pacific. *Climatic Change*, **119**, 147–161, <https://doi.org/10.1007/s10584-012-0603-5>.
- Cao, J., and B. Wang, 2019: NUIST NESMv3 model output prepared for CMIP6 CMIP. Earth System Grid Federation, accessed June 2020, <https://doi.org/10.22033/ESGF/CMIP6.2021>.
- Chen, H.-P.J.-Q. Sun, 2013: How large precipitation changes over global monsoon regions by CMIP5 models? *Atmos. Oceanic Sci. Lett.* **6**:306–311, <https://doi.org/10.1080/16742834.2013.11447099>.
- Chen, Z., T. Zhou, L. Zhang, X. Chen, W. Zhang, and J. Jiang, 2020: Global land monsoon precipitation changes in CMIP6 projections. *Geophys. Res. Lett.*, **47**, e2019GL086902, <https://doi.org/10.1029/2019GL086902>.
- Chou, C., and J. D. Neelin, 2001: Mechanisms limiting the southward extent of the South American summer monsoon. *Geophys. Res. Lett.*, **28**, 2433–2436, <https://doi.org/10.1029/2000GL012138>.
- , and —, 2003: Mechanisms limiting the northward extent of the northern summer monsoons over North America, Asia, and Africa. *J. Climate*, **16**, 406–425, [https://doi.org/10.1175/1520-0442\(2003\)016<0406:MLTNEO>2.0.CO;2](https://doi.org/10.1175/1520-0442(2003)016<0406:MLTNEO>2.0.CO;2).
- , and —, 2004: Mechanisms of global warming impacts on regional tropical precipitation. *J. Climate*, **17**, 2688–2701, [https://doi.org/10.1175/1520-0442\(2004\)017<2688:MOGWIO>2.0.CO;2](https://doi.org/10.1175/1520-0442(2004)017<2688:MOGWIO>2.0.CO;2).
- , —, and H. Su, 2001: Ocean–atmosphere–land feedbacks in an idealized monsoon. *Quart. J. Roy. Meteor. Soc.*, **127**, 1869–1891, <https://doi.org/10.1002/qj.49712757602>.
- Cook, B. I., and R. Seager, 2013: The response of the North American monsoon to increased greenhouse gas forcing. *J. Geophys. Res. Atmos.*, **118**, 1690–1699, <https://doi.org/10.1002/jgrd.50111>.
- Creese, A., and R. Washington, 2018: A process-based assessment of CMIP5 rainfall in the Congo basin: The September–November rainy season. *J. Climate*, **31**, 7417–7439, <https://doi.org/10.1175/JCLI-D-17-0818.1>.
- Danabasoglu, G., 2019a: NCAR CESM2 model output prepared for CMIP6 CMIP Historical. Earth System Grid Federation, accessed June 2020, <https://doi.org/10.22033/ESGF/CMIP6.7627>.
- , 2019b: NCAR CESM2-WACCM model output prepared for CMIP6 CMIP. Earth System Grid Federation, accessed June 2020, <https://doi.org/10.22033/ESGF/CMIP6.10024>.
- Derbyshire, S. H., I. Beau, P. Bechtold, J.-Y. Grandpeix, J.-M. Piriou, J.-L. Redelsperger, and P. M. M. Soares, 2004: Sensitivity of moist convection to environmental humidity. *Quart. J. Roy. Meteor. Soc.*, **130**, 3055–3079, <https://doi.org/10.1256/qj.03.130>.
- Emanuel, K. A., J. David Neelin, and C. S. Bretherton, 1994: On large-scale circulations in convecting atmospheres. *Quart. J. Roy. Meteor. Soc.*, **120**, 1111–1143, <https://doi.org/10.1002/qj.49712051902>.
- Fan, F., M. E. Mann, S. Lee, and J. L. Evans, 2012: Future changes in the South Asian summer monsoon: An analysis of the CMIP3 multimodel projections. *J. Climate*, **25**, 3909–3928, <https://doi.org/10.1175/JCLI-D-11-00133.1>.
- Fiedler, S., and Coauthors, 2020: Simulated tropical precipitation assessed across three major phases of the Coupled Model Intercomparison Project (CMIP). *Mon. Wea. Rev.*, **148**, 3653–3680, <https://doi.org/10.1175/MWR-D-19-0404.1>.
- Funk, C., and Coauthors, 2015: The Climate Hazards Infrared Precipitation with Stations—A new environmental record for monitoring extremes. *Sci. Data*, **2**, 150066, <https://doi.org/10.1038/sdata.2015.66>.
- Gaetani, M., C. Flamant, S. Bastin, S. Janicot, C. Lavaysse, F. Hourdin, P. Braconnot, and S. Bony, 2017: West African monsoon dynamics and precipitation: The competition between global SST warming and CO₂ increase in CMIP5 idealized simulations. *Climate Dyn.*, **48**, 1353–1373, <https://doi.org/10.1007/s00382-016-3146-z>.
- Geil, K. L., Y. L. Serra, and X. Zeng, 2013: Assessment of CMIP5 model simulations of the North American monsoon system. *J. Climate*, **26**, 8787–8801, <https://doi.org/10.1175/JCLI-D-13-00044.1>.
- Giannini, A., 2010: Mechanisms of climate change in the semiarid African Sahel: The local view. *J. Climate*, **23**, 743–756, <https://doi.org/10.1175/2009JCLI3123.1>.
- Grose, M. R., and Coauthors, 2014: Assessment of the CMIP5 global climate model simulations of the western tropical Pacific climate system and comparison to CMIP3. *Int. J. Climatol.*, **34**, 3382–3399, <https://doi.org/10.1002/joc.3916>.
- Gulizia, C., and I. Camilloni, 2015: Comparative analysis of the ability of a set of CMIP3 and CMIP5 global climate models to represent precipitation in South America. *Int. J. Climatol.*, **35**, 583–595, <https://doi.org/10.1002/joc.4005>.
- Guo, H., and Coauthors, 2018: NOAA-GFDL GFDL-CM4 model output. Earth System Grid Federation, accessed June 2020, <https://doi.org/10.22033/ESGF/CMIP6.1402>.
- Gusain, A., S. Ghosh, and S. Karmakar, 2020: Added value of CMIP6 over CMIP5 models in simulating Indian summer monsoon rainfall. *Atmos. Res.*, **232**, 104680, <https://doi.org/10.1016/j.atmosres.2019.104680>.
- Ha, K., S. Moon, A. Timmermann, and D. Kim, 2020: Future changes of summer monsoon characteristics and evaporative demand over Asia in CMIP6 simulations. *Geophys. Res. Lett.*, **47**, e2020GL087492, <https://doi.org/10.1029/2020GL087492>.
- He, C., T. Li, and W. Zhou, 2020: Drier North American monsoon in contrast to Asian–African monsoon under global warming. *J. Climate*, **33**, 9801–9816, <https://doi.org/10.1175/JCLI-D-20-0189.1>.
- Held, I. M., and B. J. Soden, 2006: Robust responses of the hydrological cycle to global warming. *J. Climate*, **19**, 5686–5699, <https://doi.org/10.1175/JCLI3990.1>.
- Hersbach, H., and Coauthors, 2020: The ERA5 global reanalysis. *Quart. J. Roy. Meteor. Soc.*, **146**, 1999–2049, <https://doi.org/10.1002/qj.3803>.
- Hsu, P., T. Li, H. Murakami, and A. Kitoh, 2013: Future change of the global monsoon revealed from 19 CMIP5 models. *J. Geophys. Res. Atmos.*, **118**, 1247–1260, <https://doi.org/10.1002/jgrd.50145>.
- Huffman, G. J., and Coauthors, 2007: The TRMM Multisatellite Precipitation Analysis (TMPA): Quasi-global, multiyear, combined-sensor precipitation estimates at fine scales. *J. Hydrometeorol.*, **8**, 38–55, <https://doi.org/10.1175/JHM560.1>.
- Hwang, Y.-T., and D. M. W. Frierson, 2010: Increasing atmospheric poleward energy transport with global warming. *Geophys. Res. Lett.*, **37**, L24807, <https://doi.org/10.1029/2010GL045440>.

- Jiang, D., and Z. Tian, 2013: East Asian monsoon change for the 21st century: Results of CMIP3 and CMIP5 models. *Chin. Sci. Bull.*, **58**, 1427–1435, <https://doi.org/10.1007/s11434-012-5533-0>.
- Jin, C., B. Wang, and J. Liu, 2020: Future changes and controlling factors of the eight regional monsoons projected by CMIP6 models. *J. Climate*, **33**, 9307–9326, <https://doi.org/10.1175/JCLI-D-20-0236.1>.
- Joetzjer, E., H. Douville, C. Delire, and P. Caias, 2013: Present-day and future Amazonian precipitation in global climate models: CMIP5 versus CMIP3. *Climate Dyn.*, **41**, 2921–2936, <https://doi.org/10.1007/s00382-012-1644-1>.
- Jones, C., and L. M. V. Carvalho, 2013: Climate change in the South American monsoon system: Present climate and CMIP5 projections. *J. Climate*, **26**, 6660–6678, <https://doi.org/10.1175/JCLI-D-12-00412.1>.
- Jourdain, N. C., A. Sen Gupta, A. S. Taschetto, C. C. Ummenhofer, A. F. Moise, and K. Ashok, 2013: The Indo-Australian monsoon and its relationship to ENSO and IOD in reanalysis data and the CMIP3/CMIP5 simulations. *Climate Dyn.*, **41**, 3073–3102, <https://doi.org/10.1007/s00382-013-1676-1>.
- Kang, S. M., I. M. Held, D. M. W. Frierson, and M. Zhao, 2008: The response of the ITCZ to extratropical thermal forcing: Idealized slab-ocean experiments with a GCM. *J. Climate*, **21**, 3521–3532, <https://doi.org/10.1175/2007JCLI2146.1>.
- Kim, H.-J., B. Wang, and Q. Ding, 2008: The global monsoon variability simulated by CMIP3 coupled climate models. *J. Climate*, **21**, 5271–5294, <https://doi.org/10.1175/2008JCLI2041.1>.
- Krasting, J. P., and Coauthors, 2018: NOAA-GFDL GFDL-ESM4 model output prepared for CMIP6 CMIP Historical. Earth System Grid Federation, accessed June 2020, <https://doi.org/10.22033/ESGF/CMIP6.8597>.
- Kriegler, E., and Coauthors, 2017: Fossil-fueled development (SSP5): An energy and resource intensive scenario for the 21st century. *Global Environ. Change*, **42**, 297–315, <https://doi.org/10.1016/j.gloenvcha.2016.05.015>.
- Kusunoki, S., and O. Arakawa, 2015: Are CMIP5 models better than CMIP3 models in simulating precipitation over East Asia? *J. Climate*, **28**, 5601–5621, <https://doi.org/10.1175/JCLI-D-14-00585.1>.
- Lambert, S. J., and G. J. Boer, 2001: CMIP1 evaluation and intercomparison of coupled climate models. *Climate Dyn.*, **17**, 83–106, <https://doi.org/10.1007/PL00013736>.
- Lee, J.-Y., and B. Wang, 2014: Future change of global monsoon in the CMIP5. *Climate Dyn.*, **42**, 101–119, <https://doi.org/10.1007/s00382-012-1564-0>.
- Li, G., and S.-P. Xie, 2014: Tropical biases in CMIP5 multimodel ensemble: The excessive equatorial Pacific cold tongue and double ITCZ problems. *J. Climate*, **27**, 1765–1780, <https://doi.org/10.1175/JCLI-D-13-00337.1>.
- Li, X., M. Ting, C. Li, and N. Henderson, 2015: Mechanisms of Asian summer monsoon changes in response to anthropogenic forcing in CMIP5 models. *J. Climate*, **28**, 4107–4125, <https://doi.org/10.1175/JCLI-D-14-00559.1>.
- Liebmann, B., and J. A. Marengo, 2001: Interannual variability of the rainy season and rainfall in the Brazilian Amazon basin. *J. Climate*, **14**, 4308–4318, [https://doi.org/10.1175/1520-0442\(2001\)014<4308:IVOTRS>2.0.CO;2](https://doi.org/10.1175/1520-0442(2001)014<4308:IVOTRS>2.0.CO;2).
- Maloney, E. D., and Coauthors, 2014: North American climate in CMIP5 experiments: Part III: Assessment of twenty-first-century projections. *J. Climate*, **27**, 2230–2270, <https://doi.org/10.1175/JCLI-D-13-00273.1>.
- Menon, A., A. Levermann, J. Schewe, J. Lehmann, and K. Frieler, 2013: Consistent increase in Indian monsoon rainfall and its variability across CMIP-5 models. *Earth Syst. Dyn.*, **4**, 287–300, <https://doi.org/10.5194/esd-4-287-2013>.
- Merlis, T. M., and M. Henry, 2018: Simple estimates of polar amplification in moist diffusive energy balance models. *J. Climate*, **31**, 5811–5824, <https://doi.org/10.1175/JCLI-D-17-0578.1>.
- Monerie, P.-A., B. Fontaine, and P. Roucou, 2012: Expected future changes in the African monsoon between 2030 and 2070 using some CMIP3 and CMIP5 models under a medium-low RCP scenario. *J. Geophys. Res. Atmos.*, **117**, D16111, <https://doi.org/10.1029/2012JD017510>.
- Moon, S., and K.-J. Ha, 2020: Future changes in monsoon duration and precipitation using CMIP6. *npj Climate Atmos. Sci.*, **3**, 45, <https://doi.org/10.1038/s41612-020-00151-w>.
- Narsey, S. Y., J. R. Brown, R. A. Colman, F. Delage, S. B. Power, A. F. Moise, and H. Zhang, 2020: Climate change projections for the Australian monsoon from CMIP6 models. *Geophys. Res. Lett.*, **47**, e2019GL086816, <https://doi.org/10.1029/2019GL086816>.
- Neelin, J. D., 2007: Moist dynamics of tropical convection zones in monsoons, teleconnections and global warming. *The Global Circulation of the Atmosphere*, T. Schneider and A. Sobel, Eds., Princeton University Press, 385 pp.
- , and I. M. Held, 1987: Modeling tropical convergence based on the moist static energy budget. *Mon. Wea. Rev.*, **115**, 3–12, [https://doi.org/10.1175/1520-0493\(1987\)115<0003:MTCBOT>2.0.CO;2](https://doi.org/10.1175/1520-0493(1987)115<0003:MTCBOT>2.0.CO;2).
- Nie, J., W. R. Boos, and Z. Kuang, 2010: Observational evaluation of a convective quasi-equilibrium view of monsoons. *J. Climate*, **23**, 4416–4428, <https://doi.org/10.1175/2010JCLI3505.1>.
- Niznik, M. J., B. R. Lintner, A. J. Matthews, and M. J. Widlansky, 2015: The role of tropical–extratropical interaction and synoptic variability in maintaining the South Pacific convergence zone in CMIP5 models. *J. Climate*, **28**, 3353–3374, <https://doi.org/10.1175/JCLI-D-14-00527.1>.
- Oueslati, B., and G. Bellon, 2015: The double ITCZ bias in CMIP5 models: Interaction between SST, large-scale circulation and precipitation. *Climate Dyn.*, **44**, 585–607, <https://doi.org/10.1007/s00382-015-2468-6>.
- Parker, D. J., P. Willetts, C. Birch, A. G. Turner, J. H. Marsham, C. M. Taylor, S. Kolusu, and G. M. Martin, 2016: The interaction of moist convection and mid-level dry air in the advance of the onset of the Indian monsoon. *Quart. J. Roy. Meteor. Soc.*, **142**, 2256–2272, <https://doi.org/10.1002/qj.2815>.
- Peterson, H. G., and W. R. Boos, 2020: Feedbacks and eddy diffusivity in an energy balance model of tropical rainfall shifts. *npj Climate Atmos. Sci.*, **3**, 11, <https://doi.org/10.1038/s41612-020-0114-4>.
- Qing, B., 2012: Projected changes in Asian summer monsoon in RCP scenarios of CMIP5. *Atmos. Oceanic Sci. Lett.*, **5**, 43–48, <https://doi.org/10.1080/16742834.2012.11446959>.
- Ramsay, H. A., and A. H. Sobel, 2011: Effects of relative and absolute sea surface temperature on tropical cyclone potential intensity using a single-column model. *J. Climate*, **24**, 183–193, <https://doi.org/10.1175/2010JCLI3690.1>.
- Riahi, K., and Coauthors, 2017: The Shared Socioeconomic Pathways and their energy, land use, and greenhouse gas emissions implications: An overview. *Global Environ. Change*, **42**, 153–168, <https://doi.org/10.1016/j.gloenvcha.2016.05.009>.
- Rienecker, M. M., and Coauthors, 2012: Atmospheric reanalyses—Recent progress and prospects for the future. NASA Tech. Rep. Series on Global Modeling and Data Assimilation, NASA/TM-2012-104606, Vol. 29, 48 pp., <http://gmao.gsfc.nasa.gov/pubs/docs/NASATM2012-104606v29.pdf>.

- Roehrig, R., D. Bouniol, F. Guichard, F. Hourdin, and J.-L. Redelsperger, 2013: The present and future of the West African monsoon: A process-oriented assessment of CMIP5 simulations along the AMMA transect. *J. Climate*, **26**, 6471–6505, <https://doi.org/10.1175/JCLI-D-12-00505.1>.
- Schneider, T., T. Bischoff, and G. H. Haug, 2014: Migrations and dynamics of the intertropical convergence zone. *Nature*, **513**, 45–53, <https://doi.org/10.1038/nature13636>.
- Séférian, R., 2018: CNRM-CERFACS CNRM-ESM2-1 Model Output Prepared for CMIP6 CMIP Historical. Earth System Grid Federation, accessed June 2020, <https://doi.org/10.22033/ESGF/CMIP6.4068>.
- , and Coauthors, 2016: Development and evaluation of CNRM Earth system model—CNRM-ESM1. *Geosci. Model Dev.*, **9**, 1423–1453, <https://doi.org/10.5194/gmd-9-1423-2016>.
- Seo, K.-H., J. Ok, J.-H. Son, and D.-H. Cha, 2013: Assessing future changes in the East Asian summer monsoon using CMIP5 coupled models. *J. Climate*, **26**, 7662–7675, <https://doi.org/10.1175/JCLI-D-12-00694.1>.
- Seth, A., M. Rojas, and S. A. Rauscher, 2010: CMIP3 projected changes in the annual cycle of the South American monsoon. *Climatic Change*, **98**, 331–357, <https://doi.org/10.1007/s10584-009-9736-6>.
- , —, S. A. Rauscher, M. Rojas, A. Giannini, and S. J. Camargo, 2011: Enhanced spring convective barrier for monsoons in a warmer world? *Climatic Change*, **104**, 403–414, <https://doi.org/10.1007/s10584-010-9973-8>.
- , —, M. Biasutti, A. Giannini, S. J. Camargo, and M. Rojas, 2013: CMIP5 projected changes in the annual cycle of precipitation in monsoon regions. *J. Climate*, **26**, 7328–7351, <https://doi.org/10.1175/JCLI-D-12-00726.1>.
- Sharmila, S., S. Joseph, A. K. Sahai, S. Abhilash, and R. Chattopadhyay, 2015: Future projection of Indian summer monsoon variability under climate change scenario: An assessment from CMIP5 climate models. *Global Planet. Change*, **124**, 62–78, <https://doi.org/10.1016/j.gloplacha.2014.11.004>.
- Sheffield, J., and Coauthors, 2013: North American climate in CMIP5 experiments. Part I: Evaluation of historical simulations of continental and regional climatology. *J. Climate*, **26**, 9209–9245, <https://doi.org/10.1175/JCLI-D-12-00592.1>.
- Song, F., and T. Zhou, 2014: Interannual variability of East Asian summer monsoon simulated by CMIP3 and CMIP5 AGCMs: Skill dependence on Indian Ocean–western Pacific anticyclone teleconnection. *J. Climate*, **27**, 1679–1697, <https://doi.org/10.1175/JCLI-D-13-00248.1>.
- Sooraj, K. P., P. Terray, and M. Mujumdar, 2015: Global warming and the weakening of the Asian summer monsoon circulation: Assessments from the CMIP5 models. *Climate Dyn.*, **45**, 233–252, <https://doi.org/10.1007/s00382-014-2257-7>.
- Sperber, K. R., H. Annamalai, I.-S. Kang, A. Kitoh, A. Moise, A. Turner, B. Wang, and T. Zhou, 2013: The Asian summer monsoon: An intercomparison of CMIP5 vs. CMIP3 simulations of the late 20th century. *Climate Dyn.*, **41**, 2711–2744, <https://doi.org/10.1007/s00382-012-1607-6>.
- Swanson, K. L., 2008: Nonlocality of Atlantic tropical cyclone intensities. *Geochem. Geophys. Geosyst.*, **9**, Q04V01, <https://doi.org/10.1029/2007GC001844>.
- Swart, N. C., and Coauthors, 2019: The Canadian Earth System Model version 5 (CanESM5.0.3). *Geosci. Model Dev.*, **12**, 4823–4873, <https://doi.org/10.5194/gmd-12-4823-2019>.
- Tian, B., and X. Dong, 2020: The double-ITCZ bias in CMIP3, CMIP5, and CMIP6 models based on annual mean precipitation. *Geophys. Res. Lett.*, **47**, e2020GL087232, <https://doi.org/10.1029/2020GL087232>.
- Vecchi, G. A., and B. J. Soden, 2007: Effect of remote sea surface temperature change on tropical cyclone potential intensity. *Nature*, **450**, 1066–1070, <https://doi.org/10.1038/nature06423>.
- Vera, C., and G. Silvestri, 2009: Precipitation interannual variability in South America from the WCRP-CMIP3 multi-model dataset. *Climate Dyn.*, **32**, 1003–1014, <https://doi.org/10.1007/s00382-009-0534-7>.
- , —, B. Liebmann, and P. González, 2006: Climate change scenarios for seasonal precipitation in South America from IPCC-AR4 models. *Geophys. Res. Lett.*, **33**, L13707, <https://doi.org/10.1029/2006GL025759>.
- Voldoire, A., 2018: CMIP6 simulations of the CNRM-CERFACS based on CNRM-CM6-1 model for CMIP experiment historical. Earth System Grid Federation, accessed June 2020, <https://doi.org/10.22033/ESGF/CMIP6.4066>.
- , and Coauthors, 2019: Evaluation of CMIP6 DECK experiments with CNRM-CM6-1. *J. Adv. Model. Earth Syst.*, **11**, 2177–2213, <https://doi.org/10.1029/2019MS001683>.
- Volodin, E., and Coauthors, 2019: INM INM-CM5-0 model output prepared for CMIP6 CMIP piControl. Earth System Grid Federation, accessed June 2020, <https://doi.org/10.22033/ESGF/CMIP6.5081>.
- Wang, B., C. Jin, and J. Liu, 2020: Understanding future change of global monsoons projected by CMIP6 models. *J. Climate*, **33**, 6471–6489, <https://doi.org/10.1175/JCLI-D-19-0993.1>.
- , and Coauthors, 2021: Monsoons climate change assessment. *Bull. Amer. Meteor. Soc.*, **102**, E1–E19, <https://doi.org/10.1175/BAMS-D-19-0335.1>.
- Wu, T., and Coauthors, 2019: The Beijing Climate Center Climate System Model (BCC-CSM): The main progress from CMIP5 to CMIP6. *Geosci. Model Dev.*, **12**, 1573–1600, <https://doi.org/10.5194/gmd-12-1573-2019>.
- Xie, P., J. E. Janowiak, P. A. Arkin, R. Adler, A. Gruber, R. Ferraro, G. J. Huffman, and S. Curtis, 2003: GPCP pentad precipitation analyses: An experimental dataset based on gauge observations and satellite estimates. *J. Climate*, **16**, 2197–2214, <https://doi.org/10.1175/2769.1>.
- Xin, X., T. Wu, J. Zhang, J. Yao, and Y. Fang, 2020: Comparison of CMIP6 and CMIP5 simulations of precipitation in China and the East Asian summer monsoon. *Int. J. Climatol.*, **40**, 6423–6440, <https://doi.org/10.1002/joc.6590>.
- Yin, L., R. Fu, E. Shevliakova, and R. E. Dickinson, 2013: How well can CMIP5 simulate precipitation and its controlling processes over tropical South America? *Climate Dyn.*, **41**, 3127–3143, <https://doi.org/10.1007/s00382-012-1582-y>.
- Yukimoto, S., and Coauthors, 2019: MRI MRI-ESM2.0 model output prepared for CMIP6 CMIP. Earth System Grid Federation, accessed June 2020, <https://doi.org/10.22033/ESGF/CMIP6.621>.
- Zhang, X., H. Liu, and M. Zhang, 2015: Double ITCZ in coupled ocean–atmosphere models: From CMIP3 to CMIP5. *Geophys. Res. Lett.*, **42**, 8651–8659, <https://doi.org/10.1002/2015GL065973>.
- Zhang, Y., and S. Fueglistaler, 2020: How tropical convection couples high moist static energy over land and ocean. *Geophys. Res. Lett.*, **47**, e2019GL086387, <https://doi.org/10.1029/2019GL086387>.